BRNO UNIVERSITY OF TECHNOLOGY

Faculty of Electrical Engineering
and Communication

MASTER'S THESIS

Brno, 2016 Bc. Michaela Fendrychová

BRNO UNIVERSITY OF TECHNOLOGY
VYSOKÉ UČENÍ TECHNICKÉ V BRNĚ

FACULTY OF ELECTRICAL ENGINEERING AND COMMUNICATION
FAKULTA ELEKTROTECHNIKY
A KOMUNIKAČNÍCH TECHNOLOGIÍ

DEPARTMENT OF ELECTRICAL POWER ENGINEERING
ÚSTAV ELEKTROENERGETIKY

ARC FAULT DETECTION
DETEKCE ELEKTRICKÉHO OBLOUKU

MASTER'S THESIS
DIPLOMOVÁ PRÁCE

AUTHOR — Bc. Michaela Fendrychová
AUTOR PRÁCE

SUPERVISOR — doc. Ing. Jaroslava Orságová, Ph.D.
VEDOUCÍ PRÁCE

BRNO 2016

VYSOKÉ UČENÍ TECHNICKÉ V BRNĚ
FAKULTA ELEKTROTECHNIKY A KOMUNIKAČNÍCH TECHNOLOGIÍ

Diplomová práce

magisterský navazující studijní obor **Elektroenergetika**
Ústav elektroenergetiky

Studentka: Bc. Michaela Fendrychová ***ID:*** 140225
Ročník: 2 ***Akademický rok:*** 2015/16

NÁZEV TÉMATU:

Detekce elektrického oblouku

POKYNY PRO VYPRACOVÁNÍ:

1. Popsat relevantní normy pro detekci střídavého elektrického oblouku v domovních instalacích a pro detekci stejnosměrného oblouku v nízkonapěťových aplikacích.
2. Provést rešerši možných postupů použitelných pro detekci střídavého oblouku v domovních elektrických instalacích v EU a USA a pro detekci stejnosměrného oblouku v nízkonapěťových aplikacích.
3. Popsat relevantní metody zpracování signálů pro účely detekce oblouku.
4. Změřit a signálově zpracovat signály elektrických oblouků (rychlá Fourierova transformace, vlnková transformace).
5. Na základě dosažených výsledků popsat algoritmus pro detekci elektrických oblouků popsaných v diplomové práci.

DOPORUČENÁ LITERATURA:

podle pokynů vedoucího práce

Termín zadání: 8.2.2016 ***Termín odevzdání:*** 20.5.2016

Vedoucí práce: doc. Ing. Jaroslava Orságová, Ph.D.
Konzultant diplomové práce:

doc. Ing. Petr Toman, Ph.D., *předseda oborové rady*

ABSTRACT

The thesis aims to analyze arc faults in the time, frequency, and mixed time-frequency domains in order to identify methods suitable for the detection arc faults in both AC and DC systems. Current standards in the field of arc fault detection are briefly introduced. Standardized tests according to the IEC 62606:2013 and UL 1699B have been performed to acquire arc fault signal data. Due to the insufficiency of the present standardized testing methods, a novel arc ignition technique based on springed wire is introduced. The obtained data have been analyzed in the time, frequency, and mixed time-frequency domains using the FFT, SFTF, and Wavelet transform. Based on the performed survey of published detection methods and considering the findings, observations, and experience generated during the performed signal analyzes, a detection method applicable in both the AC and DC systems and exploiting the Wavelet transform is proposed.

KEYWORDS

Arc fault, Arc fault detection, Time domain, Frequency domain, Fourier transform, Short time Fourier transform, Wavelet transform, AFDD

ABSTRAKT

Diplomová práce je zaměřena na problematiku analýzy signálů za účelem detekce poruchového oblouku, přičemž analýza signálů je prováděna v časové, frekvenční a smíšené časově-frekvenční oblasti. Práce stručně shrnuje existující normy pro zařízení pro detekci poruchového oblouku. Práce dokumentuje testy a měření, které byly realizovány v souladu s normami IEC 62606:2013 a UL 1699B. Z důvodu nedostatečnosti stávajících norem je v práci popsána nová metoda iniciace poruchového oblouku. Naměřená data byla analyzována s využitím rychlé Fourierovy transformace, krátkodobé Fourierovy transformace a vlnkové transformace. Na základě provedeného literárního průzkumu a s využitím výsledků provedených analýz signálu je v práci proveden návrh nové detekční metody pro účely detekce poruchového oblouku v systémech napájených střídavým i stejnosměrným napětím.

KLÍČOVÁ SLOVA

Poruchový oblouk, Detekce poruchového oblouku, Časová oblast, Frekvenční oblast, Fourierova transformace, Krátkodobá Fourierova transformace, Vlnková transformace, Oblouková ochrana

FENDRYCHOVÁ, Michaela *Arc Fault Detection*: master's thesis. Brno: Brno University of Technology, Faculty of Electrical Engineering and Communication, Department of Electrical Power Engineering, 2016. 85 p. Supervised by doc. Ing. Jaroslava Orságová, Ph.D.

DECLARATION

I declare that I have written the Master's thesis titled "Arc Fault Detection" independently, under the guidance of the supervisor, and using exclusively the technical references and other sources of information cited in the thesis and listed in the related comprehensive bibliography at the end of the thesis.

As the author I furthermore declare that, with respect to the creation of this Master's thesis, I have not infringed any copyright or violated anyone's personal and/or ownership rights. In this context, I am fully aware of the consequences of breaking Regulation § 11 of the Copyright Act No. 121/2000 Coll. of the Czech Republic, as amended, and of any breach of rights related to intellectual property or intruduced within amendments to relevant Acts such as the Intellectual Property Act or the Criminal Code, Act No. 40/2009 Coll., Section 2, Head VI, Part 4.

Brno ....

author's signature

ACKNOWLEDGEMENT

I would like to express my gratitude to my colleagues at Eaton Corporation - Menomonee Falls Innovation Center, U.S.A. and at The Eaton European Innovation Center (EEIC) in Prague. Special thanks go to Steve Schmalz and Dale Gass. Their guidance, support and patience during my stay in Menomonee Falls Innovation Center were crucial for elaboration of my thesis. Furthermore I would like to thank to Engelbert Hetzmannseder. Without his support, open mind and enthusiasm my Internship at Eaton Corporation would have not been possible. I also would like to express my gratitude to doc. Ing. Jaroslava Orságová, Ph.D., who was my academic supervisor, for both administration of my thesis, for comments and remarks that helped to improve my thesis and for willingness to administer diploma work in a foreign language.

Brno ....

author's signature

CONTENTS

LIST OF FIGURES

LIST OF TABLES

1 INTRODUCTION

Electricity can cause damage to property, and its effect can also result in injuries and deaths. To minimize the risks associated with the production, distribution, and use of electric energy, various precautions based on hazard analysis are used. The major electricity related hazards as stated in [17] are:

- Electric shock from contact with live parts;
- Contact burns;
- Injury from exposure to arcing;
- Fire from faulty equipment and installations;
- Explosions caused by an unsuitable electrical apparatus;
- Explosions caused by ignition of flammable vapors or dusts.

In electric installations, various protection devices and technologies are used to reduce the hazards listed above. The most common protective instruments are circuit breakers, which minimize the hazards related to short circuits and overload, and residual current devices (also known as ground fault circuit interrupters) to detect dangerous leakage currents. Medium sensitivity residual current devices (RCDs) are used to detect the leakage current, an effect capable of causing fires, while high sensitivity RCDs are designed to prevent both fires, injuries, or loss of life. The IEC has proposed preferred values of rated residual currents for the RCDs [1]:

Sensitivity	*Preferred values*	*Protection*
High	6 mA / 10 mA / 30 mA	Life & injury protection
Medium	100 mA / 300 mA / 500 mA / 1000 mA	Fire protection
Low	3 A / 10 A / 30 A	Machine protection

Tab. 1.1: RCD sensitivity levels according to the IEC

1.1 Motivation for Arc Fault Detection

While RCDs with tripping current not exceeding 300 mA are required for fire prevention (e.g., IEC 60364-4-482), currents as low as 50 -– 100 mA have been found capable of inducing ignition and fire as a result of surface tracking on the insulation [6].

Sufficiently sensitive RCDs are efficient in fire risk reduction by detecting leakage currents and arcing to ground as a consequence of tracking currents within an electrical installation. However, neither the RCDs nor the circuit-breakers are able to cope with the risk of electrical fire due to series or parallel arcing between live

conductors. The IEC is well aware of this fact, as is obvious from the following citation [6]:

> *"Experience and information available confirmed that the r.m.s. current value of an earth fault current caused by an arcing fault, which is able to ignite a fire, is not limited to the rated power supply frequency of 50/60 Hz, but may contain a much higher frequency spectrum that is not taken into account for the testing of RCDs."*

Based on the above-described limitations of existing protection devices, there is a market niche for protection devices that would facilitate the reduction of hazards related to:

- Serial and parallel arcing,
- Cases of arcing between live conductors and ground that are beyond the detection abilities of fire protection and device protection RCDs.

To be able to quantify the significance of risks associated with the above-outlined hazards, risk analysis based on the statistical evaluation of the consequences of arcing is needed.

1.2 Consequences of Arcing in Electrical Installations

Electrical arcing is a powerful physical phenomenon which can lead to significant damages and consequent losses. An electric arc consists of ionized gas (plasma), and therefore its temperature is between 6 000 K and 20 000 K [34]. Depending on the location of arcing and its surroundings, there are three types of potential undesirable outcomes of arcing:

1. Destruction of all insulators in close proximity to the electric arc;
2. Destruction of the electrical contacts or conductors that take part in arcing;
3. Destruction of the device where arcing occurs or destruction of the relevant part of electric wiring.

All these types of failures can induce very fast ignition of the surrounding combustibles. The rate of the occurrence of fires caused by electric arcs can be estimated based on published fire statistics, where fire causes are provided.

1.3 Statistical Data

1.3.1 AC Grid

> *"In 2006 the United States Fire Administration (USFA), a part of the Department of Homeland Security, reported that 67,800 residential fires were related to electrical problems resulting in 485 deaths, over 2,300 injuries and $868 million in property losses. The USFA also states that home electrical wiring causes twice as many fires as electrical appliances."* [31]

In Figure 1.1 we can observe that the average loss per structure fire in the US is increasing; this means even if the overall number of fires is decreasing, possibly due to the compulsory installation of RCBs in new or renovated housings, the average damage per fire is rising. Thus, the importance of the ability to detect hazardous events before they can lead to disastrous consequences is also on the increase.

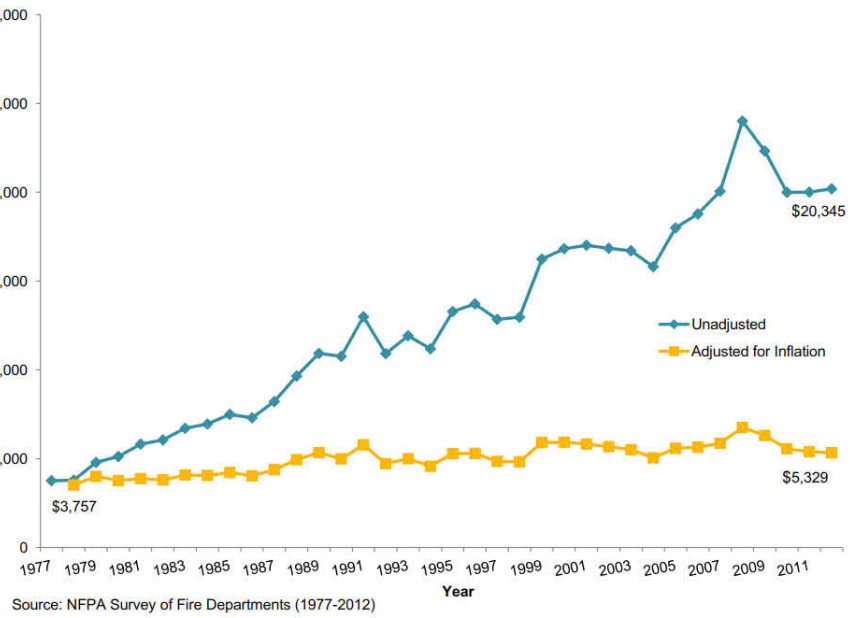

Fig. 1.1: The average loss per structure fire in the United States (1977-2012) [19].

In Europe, it is estimated that 60 % of apartment blocks are older than 30 years, and this number grows by 1 % annually. Only 0.32 % of apartment blocks are renovated every year. Consequently, the electrical installations are becoming increasingly older, and the risk of a fire is progressively higher [38].

In the South Bohemian region (population of 600,000), nineteen fires were ignited by electrical arcing between 2009 and 2013. These fires constitute approximately 4 % of all related accidents where electricity was reported as a cause. As shown in

Fig 1.2, the number of fires ignited by electrical arcing is rapidly increasing. While in the year 2009 these fires made up 0.09 % of all fires, in the year 2013 they already amounted to 0.74 % of all fires [7].

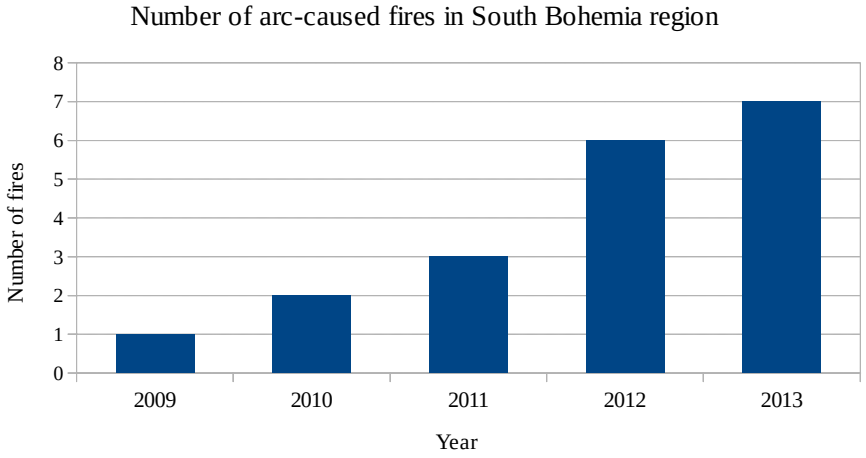

Fig. 1.2: The number of fires ignited by electrical arcing in South Bohemia between 2009 and 2013; adopted from [7].

1.3.2 DC Grid

In recent years, probably due to the advances in power electronics that enable highly efficient AC/DC and DC/DC energy conversion and thanks to photovoltaic systems, the popularity of DC systems has been rising. This is documented by the following texts:

> *"Especially since 2006, reports have claimed that fire accidents in residential, commercial, and utility PV installations happened more frequently than before. Subsequent investigation proved that most of the electrical fire arose from DC arcs."* [14]

> *"Specially due to the large number of worldwide photovoltaic installations and the increasing use of battery systems within the last years several investigations have been carried out about the reasons of reported fire incidents and initiated research programs and standard specifications."* [35]

1.4 Arc fault detection devices

Arc faults have been recognized as a cause of fires since the beginning of the 20th century; patent applications related to arc fault protection date back to the 1930s. Arc Fault Circuit Interrupters (AFCI) began to appear on the U.S. market in 1997 [33].

Although AFCI devices are well established in the North American market and the products are well-developed, nuisance tripping becomes rather complicated with new kinds of loads. Moreover, new types of applications and novel application domains (e.g., electric vehicles and photovoltaic power plants) substantiate the development of novel arc detection solutions.

2 RESIDENTIAL AC LOADS AND RELATED AFDD STANDARDS

2.1 New Kinds of Loads

Older Arc Fault Detection Devices (AFDDs) are known to use one frequency band to distinguish arcing and non-arcing events. With new loads introducing high frequency noise in to the residential circuits the old simple detection approach is not robust enough and nuisance tripping starts to occur. The most influential new kinds of loads are:

Switching Power Supplies: While all switching power supplies are a source of high frequency noise, it has been observed that there are significant differences of amounts of generated noise between various power supplies. The biggest problem are small, low cost supplies.

AC Drives: AC drives (Frequency converters) use switching power electronic devices in order to change frequency and magnitude of the grid voltage to a variable load voltage, where the load is an AC motor.

Signal characteristics of real loads (old and new) are used in standardized testing of new AFDDs. Next part addresses standards from US, EU and Czech Republic.

2.2 Standards for Residential AFDD

According to the IEC 62606 the Arc Fault Detection Device (AFDD) is a device, which is intended to mitigate the effects of arcing faults by disconnecting the circuit when an arc fault is detected. The Arc Fault Detection Devices are in the US standards and consequently in the use markets called Arc Fault Circuit Interrupters (AFCIs). However, the definition of the device function is the same regardless the different designations AFDD or AFCI. The AFDD devices for residential applications have been first standardized in the US where AFDD is mandatory for all new residential electrical installations. US standard was published as UL1699 in 2006 with a revision in 2013. In the year 2013 the international standard IEC 62606:2013 has been published and national European versions like ČSN EN 62606 has followed in 2014. These two versions are almost similar. Significant differences between them will be addressed later in this chapter.

2.2.1 IEC 62606:2013

In following text there are described parts of IEC 62606:2013 standard that are important for the topic of this thesis. The relevant parts are requirements for AFDD operation in case of a series arcing and parallel arcing and prescribed testing. Also masking test for verification of correct operation is included in the description.

a) Series arc fault tests

For series arc fault tests there are two possible ways to generate an arc. First a cable specimen with parallel conductors with insulation slit and carbonized path created in between conductors). Second possibility is arc generator with one copper rod and one carbon-graphite rod serving as electrodes. One electrode is stationary and one is moving.

For an AFDD to pass the tests described in the IEC standard, it shall trip before maximum break time stated in Table 2.1 ($U_n = 230\ V$) or Table 2.2 ($U_n = 120\ V$) for each current level if the cable specimen is used for arc generation. If an arc generator is used tripping time shall not exceed 2.5 times the maximum break time.

Test arc current	2.5 A	5 A	10 A	16 A	32 A	63 A
Maximum break time	1 s	0.5 s	0.25 s	0.15 s	0.12 s	0.12 s

Tab. 2.1: Limit values of break time for $U_n = 230\ V$

Test arc current	5 A	10 A	16 A	32 A	63 A
Maximum break time	1 s	0.4 s	0.28 s	0.14 s	0.14 s

Tab. 2.2: Limit values of break time for $U_n = 120\ V$

For series arc fault there are four tests prescribed. Three tests are for sudden appearance of arcing, for inserting a load with a series arc fault and for case of closing on series arc fault. Fourth test is done to verify correct operation at temperature limits (-5 °C and 40 °C).

b) Parallel arc fault tests

For parallel arc fault there are three prescribed tests. The AFDD shall trip if the number of arcing half-cycles stated in Table 2.3 (for both $U_n = 230\ V$ and $U_n = 120\ V$) occurs within 0.5 s. The stated current is the circuit current before the arcing starts.

First test is with parallel arc with limited current. Cable specimen for this test is prepared in a same way as for series arc fault tests and the test is performed at fault current levels of 75 A and 100 A.

Test arc current	75 A	100 A	150 A	200 A	300 A	500 A
Number of half-cycles	12	10	8	8	8	8

Tab. 2.3: Maximum allowed number of arcing half-cycles within 0.5 s

Second test is parallel arcing cutting test. Test setup is the same as in case of limited current test but this time the cable specimen insulation is cut during the test with device displayed in Figure 2.1. It consists of steel blade used for cutting of the cable specimen. The cutting edge can be positioned anywhere along the specimen and a new cable specimen for each test is necessary.

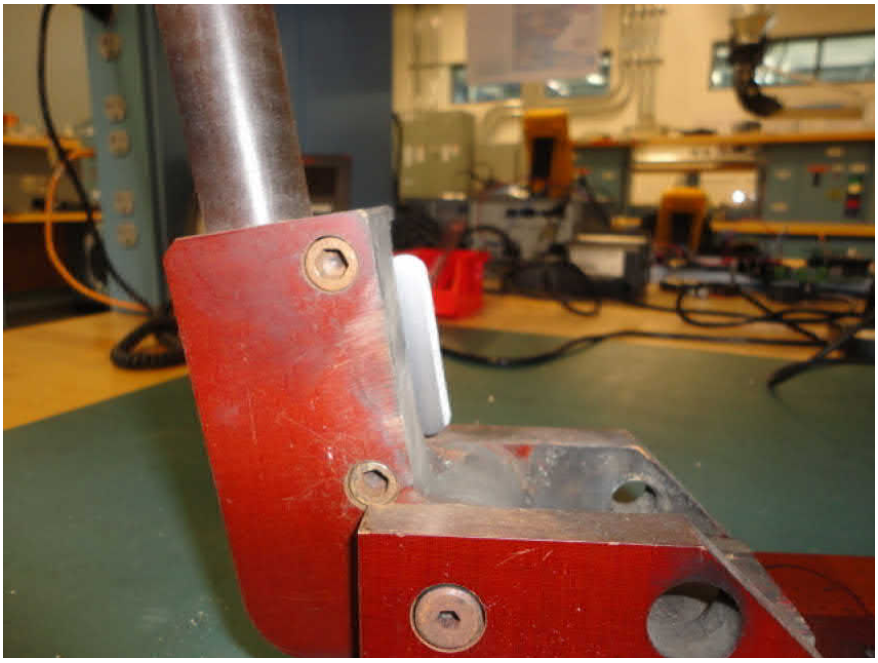

Fig. 2.1: Cutting device for Parallel arcing test

The last test is verification of correct operation in case of earth arc fault. This test is to be performed at current levels of 5 A and 75 A. For 5 A current level the tested device shall trip in accordance with Tables 2.1 and 2.2. For 75 A current level the tested device shall trip in accordance with 2.3. The test setup is the same as in the case of limited current test.

c) Masking tests

For these tests it is possible to use arc generator or carbonized cable specimen to generate arc fault. For AFDD to pass the tests it shall trip before maximum break time stated in Table 2.1 ($U_n = 230\ V$) or table 2.2 ($U_n = 120\ V$) for each current level if the cable specimen is used for arc generation. If Arc generator is used tripping time shall not exceed 2.5 times the maximum break time. There are three different

series of tests for masking tests. First is series of tests with inhibition loads. The following inhibition loads are defined in the standard:

i. A vacuum cleaner rated for 5 A and 7 A if $U_n = 230\ V$ or 10 A and 14 A if $U_n = 120\ V$, it shall be started and run.
ii. An electronic switching mode power supply with rated current at least 2.5 A if $U_n = 230\ V$ or 5 A if $U_n = 120\ V$, it shall be turned on.
iii. A capacitor start motor with peak inrush current of 65 A ±10 % if $U_n = 230\ V$ (2.2 kW capacitor motor is to be used) or 130 A ±10 % if $U_n = 120\ V$, it shall be started under load and run.
iv. An electronic lamp dimmer (thyristor type) with a filtering coil controlling tungsten load. For $U_n = 120\ V$ the dimmer is 1000 W and the load is 1000 W consisting of four 150 W bulbs and four 100 W bulbs. For $U_n = 230\ V$ the dimmer is 600 W and the load is 600 W. The dimmer is to be turned on with the dimmer preset at full on, conduction angles of 60°, 90°, 120°, and at the minimum setting that causes the lamps to ignite.
v. Fluorescent lamps 2x40 W and an additional 5 A resistive load.
vi. A 12 V halogen lamps powered with electronic transformer (total power 300 W) and an additional 5 A resistive load.
vii. A 600 W electric hand tool (drill).

Second series of tests are a masking tests with two different EMI filter loads. The last test is a test with line impedance. A branch circuit connected behind the AFDD consists of 30 m of 2.5 mm^2 armored cable (two conductors with steel armor). The maximum break times for AFDD to trip are the same as with the previous tests.

d) Unwanted Tripping Tests

This tests are done to ensure AFDD does not trip during normal operation. Two tests are performed. First one is Cross talk test and the second one is test with various disturbing loads. The later one is the same as masking test with inhibition loads only without the arc generator or cable specimen. The different loads are the same but are energized during at least 5 s. Also Start/Stop operations for each load (5) are to be done.

2.2.2 ČSN EN 62606

The difference in between IEC 62606:2013 and ČSN EN 62606 [2] is that the ČSN is written only for $U_n = 230\ V$. Apart from that the standards are same.

2.2.3 UL 1699

The UL 1699 [36] differs in many ways therefor its testing procedures are stated in following text. It is necessary to remind the reader of frequency difference. In the USA the grid frequency is 60 Hz and therefore all following described tests are rated at this frequency. There are four test sequences relevant to the topic of this thesis. These are carbonated path tests, point contact arc tests, unwanted tripping tests and operation inhibition tests.

Carbonated path tests

i. Arc ignition tests
   For this tests the cable specimen is prepared in two ways. The nonmetallic sheathed cable's insulation is to be cut around line (first test) or grounded circuit conductor (second test). The cut is to be wrapped in insulating tape. Around the tape is to be loosely wrapped in surgical cotton. The load (purely resistive) resistance is to be adjusted to 5 A. The test runs until the AFDD trips or the cotton is ignited or neither happen for 5 minutes. The test is successful if the AFDD trips before the cotton ignites.

ii. Arc interruption test
   For this test the cable specimen's insulation is to be cut around all three conductors. The AFDD shall clear an arc fault if 8 half-cycles of arcing occurs within a period of 0.5 s. The test is to be done at 75 A and 100 A current levels.

iii. Arc clearing test
   The cables specimen's insulation is to be cut around two conductors and taped with insulation tape. Then it is to be conditioned so the carbonized conductive path in between conductors is created. The current levels and required clearing times are in Table 2.4.

Test current	AFCI: 15A	AFCI: 20 A	AFCI: 30 A
5 A	1 s	1 s	1 s
10 A	0.40 s	0.40 s	0.40 s
100% rated current	0.28 s	0.20 s	0.14 s
150% rated current	0.16 s	0.11 s	0.10 s

Tab. 2.4: Arc Test Clearing Times

b) Point contact arc tests

These testing procedure is the same as cutting test in IEC 62606. The current levels

are 75 A, 100 A, 150 A, 200 A, 300 A, and 500 A. The AFDD shall clear an arc fault if 8 half-cycles of arcing occurs within a period of 0.5 s.

c) Unwanted tripping tests

There are six different test series in this part. Each test series has different type of loads. In all of these tests AFDD shall not trip. In the following text is described whole test series and basic information about the loads to be used is also provided.

i. Inrush current test

There are two different loads in this tests. The first one is a 1000 W tungsten load consisting of prescribed bulbs. A control switch shall close the circuit at 30, 60 and 90 degrees or 60 times with random closing. The second load is a capacitor start (air compressor type) motor with a peak inrush current of 130 A±10 %. The motor is to be started under load (without any air pressure in the air tank).

ii. Normal operation arcing test

This tests are done with seven different kinds of loads:

a) A vacuum cleaner rated at 10.8 – 12 A full load.
b) A bi-metallic appliance (skillet, flat iron etc.) rated 1200 W ±10 %.
c) A 1000 W tungsten load consisting of prescribed light bulbs.
d) A load c) with a general-use snap switch.
e) An electronic variable-speed electric hand-held shop tool rated 5 – 7 A.
f) A ceiling fan speed control (capacitive type with rotary switch) rated 1.5 A controlling a ceiling fan.
g) An air purifier (employing electrostatic forces to move air and containing UV lamp).

iii. Non-sinusoidal waveform test

Four loads for this tests are:

a) A 1000 W electronic lamp dimmer (thyristor type) with a filtering coil controlling a 1000 W tungsten load consisting of prescribe bulbs. A 600 W dimmer without a filtering coil controlling a 600 W tungsten load consisting of prescribed bulbs.
b) An electronic variable-speed electric hand-held shop tool rated 5 – 7 A.
c) An electronic switching mode power supply (one or more) having a total load current at 120 V of at least 5 A with minimum THD of 100 % and prescribed other minimum current harmonics.
d) Two 40 W fluorescent lamps plus an additional resistive load.

iv. Cross talk test

There are two tests with two branch circuits. One with AFDD and one with-

out. Test utilize different kinds of conductors.

v. Multiple load
   The load from non-sinusoidal waveform tests b) and d) is to be used at current equal to the AFDD rating (additional load is of resistive kind).

vi. Lamp burnout
   The device to force the incandescent (100 W) lamp to burn out is described in the standard.

d) Operation inhibition tests

In this testing sequence it is prescribed to test branch/feeder or combination AFDD with carbonized path cable specimen. For the outlet circuit, portable or cord AFDD the arc generator is prescribed. The cable specimen is to have insulation cut around the line (same as in arc ignition test). The arc generator device is the same as in IEC 62606 tests with arc generator. For this sequence there are three test series each with different kinds of loads. The test currents and required clearing times are same as for the Carbonated path tests and were provided in Table 2.4 on page 20.

The first set of tests in this group are the masking tests. The loads for this tests are a vacuum cleaner, an electronic switching mode power supply, a capacitor start motor (air compressor type), a 1000 W and a 600 W electronic lamp dimmers, and two 40 W fluorescent lamps plus additional 5 A resistive load.

The second set of tests are the tests with EMI filters. These are the same as the tests described in the IEC 62606 standard.

Third set are the tests with the line impedance. These tests are to be done with an armored cable and with a steel pipe.

3 HIGH POWER DC APPLICATION FIELDS

3.1 DC Application Fields

There are several new application fields for industrial DC AFDD technology. These are discussed below.

As mentioned in the fire safety part of this thesis, there is demand for electric arc detection in extensive photovoltaic plants, where the current levels are between 100 A and 400 A and voltage levels are between 1000 V – 1500 V. PV power plants are now mandatorily protected on string level only and this protection is based on standard UL 1699B.

After all strings are combined together, the amount of transferred power can be very high and every arcing event has disastrous consequences. The schematic of PV plant is displayed in Figure 3.1. The part protected by devices specified in UL 1699B is highlighted by green circle and the part where the new AFDD technology is intended for protection is in red circle. The part protected by the intended novel protection device is shown in green circle. At this time there are few existing devices for arc protection of the high power part of PV plant but these need to be tuned to the specific installation and universally applicable devices are not available at the market.

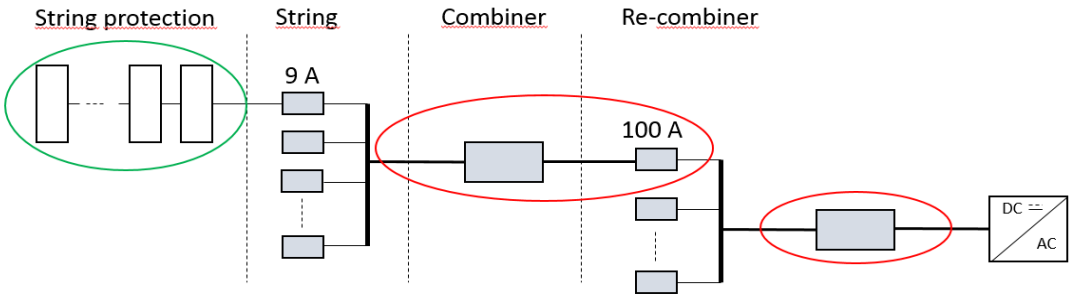

Fig. 3.1: Schematics of DC Power Plant with Highlighted Areas of Interest

Other possible application field for high power DC arc detecting devices is found in mining industry and other industries, where battery powered electric trucks are used. Next application area are shared DC links for VFD drives for oil and gas industry. And the last one potential application field is DC power distribution in large scale datacenters.

3.2 UL 1699B Standard

In the following paragraphs there are described tests, important for the topic of this thesis, in the UL 1699B standard [37]. These tests are for series and parallel arcing detection, unwanted tripping test and series arc test with high line impedance.

For all prescribed tests the same arc generator, displayed in Figure 3.2, is to be used.

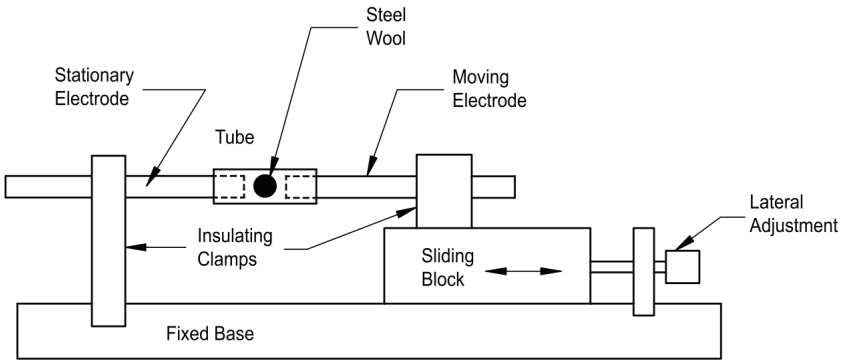

Fig. 3.2: Arc Generator as depicted in the UL 1699B Standard

The electrodes are to be made from copper 6.35 mm in diameter. The tube is to be made from polycarbonate. The dimensions are 19 mm in length, 9.5 mm outer diameter and 6.35 mm inner diameter.

Fig. 3.3: Steel Wool inside Polycarbonate Tube [4]

The arc is ignited by small amount of very fine steel wool positioned in between the electrodes as displayed in Figure 3.3. A brief description of each of the tests follows.

a) Series Arcing Detection test

The arc generator and tested device are to be connected in series to a source of

PV power. The PV modules are to be connected in a series or series-parallel. A ballasting resistor may be used to achieve the desired voltage but no inverter or charge controller is to be used. The test specifications are stated in Table 3.1.

Arcing current	Arcing voltage (approx.)	Arc Power (avg.)	Maximum time
7 A	43 V	300 W	2.0 s
7 A	71 V	500 W	1.5 s
14 A	46 V	650 W	1.2 s
14 A	64 V	900 W	0.8 s

Tab. 3.1: Tests conditions and Clearing Times according to the UL 1699B standard

b) Parallel Path Arcing Detection test

For this test the arc generator is to be connected in parallel with a load (an inverter, a converter or a charge controller). The test specifications are the same as in the previous case.

c) Unwanted tripping test

There are two different loading conditions for this test and during the device shall not trip under both of them. The power supplied is at rated voltage and current of the device.

i. Loading Condition I is made of one of the following devices: a single-phase inverter, a three-phase inverter, a converter or a charge controller.
ii. Loading Condition II is DC switching test with an inverter as the load.

d) Operation Inhibition test

The same series of tests as for series arcing test shall be performed with prescribed masking loads for the conditions of 300 W and 900 W. The loads are PV power source and inverter wired in two different ways.

e) Line Impedance Test

The tests performed are the same as those for series arcing detection at the rates of 300 W and 900 W. The only difference is the conductor. It is to be 60.96 m in length with four 180 degree bends of 15.24 cm radius.

4 STATE OF THE ART IN THE ARC-FAULT DETECTION

The methods used in AC and DC arc–detecting algorithms are usually the same for frequency and mixed time-frequency domains. Most of the research groups use arc current signal as it is an easily obtainable signal, which carries most of the information for the arc detection. This has been verified in the signal analysis part of this thesis. The used detection approaches can be divided into four main groups:

1. Time domain signal processing;
2. Frequency domain signal processing;
3. Mixed time–frequency signal processing;
4. Arc detection based on arc models.

Often there is more than one approach combined for the detection algorithm in order to improve detection reliability and reduce nuisance tripping.

Signal characteristics in the time domain are typically used for the DC arc fault detection. The most often used characteristics for the arc detection are the current change $I_{max} - I_{min}$, change within certain time period is considered; this method is described in [42], [14], [9]. The length of the time window used in [14] is 10 ms.

In [9] the authors use the above described simple signal processing for distinction between arcing and normal operation of the loads under the assumption that the duration of abrupt changes is shorter for the arcing that for the loads operations, moreover such abrupt changes are more frequent during arcing than during normal operation.

Another common way to detect the arcing in the time domain, according to papers [15] and [26], is to use the peak-to-peak value of the current; the arc detection is then based on exceeding of a threshold value.

From the literature survey it stems, that the time domain signal processing is not common for the AC arcing detection. However, in [31] a sudden change of current value (together with a threshold value of the current signal) is used for the arc fault detection.

Arc fault detection for AC applications based on the temporal analysis is presented in [23], the methods examined there are the Kalman filter, Crest factor and "Moment mathematic algorithms".

In [27], [12] and [41] the arcing detection methods in various application fields are presented. In [27] the arc detection in 42 V car electric system is based on evaluation of the rate of change of the arc current during the arc fault, the rate of change is then compared with a threshold value. In [12] the detection of the AC arc in an aircraft electrical system is based on a signal processing of the current signal;

the current signal is filtered through a 1 kHz high pass filter. Because of the 270 V power distribution system, which is under consideration for the new aircrafts, the detection based on recognition of abrupt variations of the current (simple differential circuit was utilized for this task) is presented [41]. In that paper an FFT is also utilized to improve the detection performance.

The frequency–domain–based arc detection is usually based on Fast Fourier Transform (FFT). In [15] and [9] the increase of the current signal energy during the arcing is used. The scaled measure for the calculation of the energy change introduced in [15] is:

$$N = \frac{S_{arc} - S_{no-arc}}{S_{arc} + S_{no-arc}},$$

where the S is an absolute sum of the FFT magnitudes at specific frequency range below 10 kHz. In the paper [9] it is claimed that this approach is especially useful for detection of the arc ignition as the energy value of the signal for the established arcing is significantly lower.

In [14] the detection of the arc fault in the DC circuit is done by comparing the energy of the current in 1 – 4 kHz frequency band with a DC current component and AC current component of the signal. More demanding, in terms of the computational power, is the method used in [32], where the authors propose detection based on Discrete Fourier Transform with Hanning window used as a windowing function. In this case the signal in the 20 – 120 kHz frequency band is used and for the DFT the whole band is divided is divided into five sub-bands (20 kHz each). Papers, where authors propose detection based on wavelet transform, form a big part of recently published research papers in the field of the arc fault detection. Both AC and DC circuits are examined in those papers.

In [28] the authors compare Discrete Wavelet Transform (DWT) with Continuous Wavelet Transform (CWT) and find the first one to be superior in terms of the arc fault detection. The DWT and wavelet packet decomposition are then proposed for the signal processing. The DWT is also used in [20], [39], [25], [43], [9], [40] and [24]. The main difference among the presented DWT methods for arcing detection are the used mother wavelet functions and the applied windowing functions.

In [20], [39], [25], [43] and [40] functions from the Daubechies family are used. The other families of functions that are being used are the Haar functions in [24] and [10] and the Coiflet functions in [9]. In [10] authors try not only to detect arc faults, but also to localize it in the photovoltaic power system. They used wavelet transform, which was found to be useful for detection of the presence of the arc fault, and subsequently apply statistical methods (matched filter, zero crossing method and recurrence plot analysis) for the fault localization.

Additional wavelet transform techniques are presented in [42], [11]. In [42] the wavelet decomposition is used to obtain information about arcing. Multi-scale dyadic wavelet transform and Mallat algorithm for decomposition and reconstruction of the signals obtained in the AC circuit was used in [11] with good results for distinguishing between the arc fault and common loads.

The last group of methods for the arc fault detection are the methods based on development of models of the arcing in the electrical circuit and evaluation of difference between the outputs of the model with the signals of interest. In the paper [5] authors propose second-order auto-regressive model derived by the Burg method coupled with distance measurements for the detection. This method is claimed to be suitable for both AC and DC arc detection. In [22] monitoring of real-time correlation coefficients from one period to the other period is considered. Finally in [35] quasi-stationary large-signal model and linearized small-signal model were created and used for the arc fault detection.

5 PERFORMED MEASUREMENTS

From the survey performed in the chapter 4 it stems that in order to analyze signal patterns of the arc faults, two fundamentally different approaches are possible. Either a theoretical model of arc in an electric circuit can be developed and implemented in a simulation environment, or a real arc fault signals can be measured and analyzed.

Due to the high costs of the real measurements the modeling is a quite common approach in the arc fault research and lot of work has been done in order to create models of high quality. As good and precise the models are, the arc fault is known to be a highly variable phenomenon with so many random influences, than even the best models cannot comprehend all of its details.

Modeling of the arc fault was not used for this theses, however further reference on the modeling topic can be found either in the chapter 4 or in [20] and [35].

Approach chosen in this thesis is solely experimental and measurements on artificially created arcs using standardized test setups were performed in order to acquire arcing signal data. Broad range of tests for both AC and DC circuits were performed. In this chapter the testing methodology will be described.

5.1 DC Testing

The tests for DC application field was based on UL 1699B standard, however additional tests, which differ from the standard, have been performed as well. Complete series of UL 1699B tests has been done. The primary power source used were a PV panels, which have been connected in accordance to the standard. Signals for both current levels (7 A, 14 A) and all defined gaps have been measured. Because the intended application field exhibits much higher currents, than those prescribed in the UL 1699B, additional tests at current levels of 27 A, 50 A, and 72 A have also been carried out. The test setup used is shown in Figure 5.1. Although the depicted test setup was captured after the arcing test, the two copper electrodes and remains of the plastic tube are clearly visible. The electrodes were positioned manually.

5.1.1 UL 1699B test procedure drawbacks

It was observed that the test procedure defined in the UL 1699B exhibits several drawbacks:

- The steel wool ignites immediately after the relays close, therefore it is not possible to distinguish between transients related to powering the circuit up and transients related to ignition of the arc.

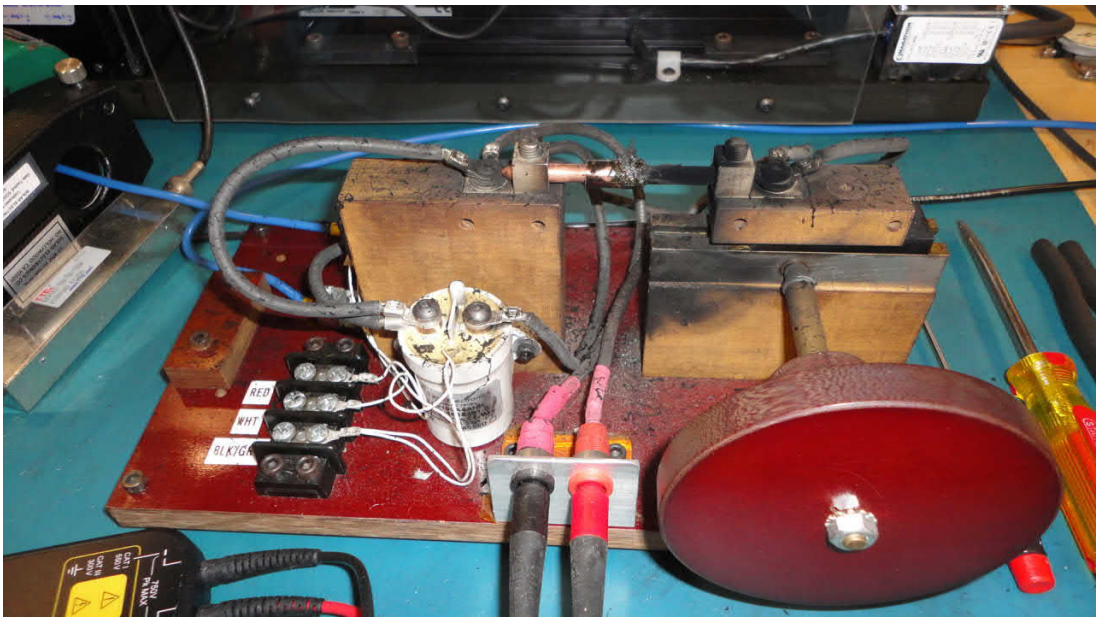

Fig. 5.1: Test Setup with exploded polycarbonate tube

- With higher currents the polycarbonate tube described in UL 1699B starts to explode, which can also be seen in Figure 5.1. The result of such explosion is splashed plastic on the test setup, which is difficult to clean, and the explosions brought up safety concerns.
- There is a significant difference between wiring of the test for lower and higher currents: the wiring at higher power levels is done with metal bus bars and screws, therefore it does not include any plastic insulation.
- The carbon particles from the polycarbonate tube make the resulting arcing more violent with more transient events when compared to arcing events when carbon particles are not present.

5.1.2 Beyond the UL 1699B: Springed wire test

In order to be able to observe the undisturbed arcing signal, it was necessary to find a way to delay the ignition of the arc, i.e. to modify the testing procedure. All of the above issues were solved by a novel approach to the arc ignition. The novel ignition method has been named *Springed wire test* because it uses thin copper wire spring as the arc generator. A thin copper wire is shaped to form a little spring. This spring, unlike the steel wool, sustains itself in between the electrodes and the plastic tube can be fully omitted. Use of copper material for the spring is not expected to be crucial, thin copper wire has been used as it is an inexpensive well standardized conductive material with good availability.

The copper wire spring is able to pass the current for sufficient period of time, before it burns out and the arc ignites. The delay between powering the circuit up and ignition of the arc enables to distinguish between transients caused by closing of the relays and transients related to the beginning of the arcing. It confirms that the events of relays closing and arc ignition are clearly separated in the measured signal. Therefore in addition to standard steel wool ignition tests, the tests, where the springed wire is used as the arc initiator, were carried on.

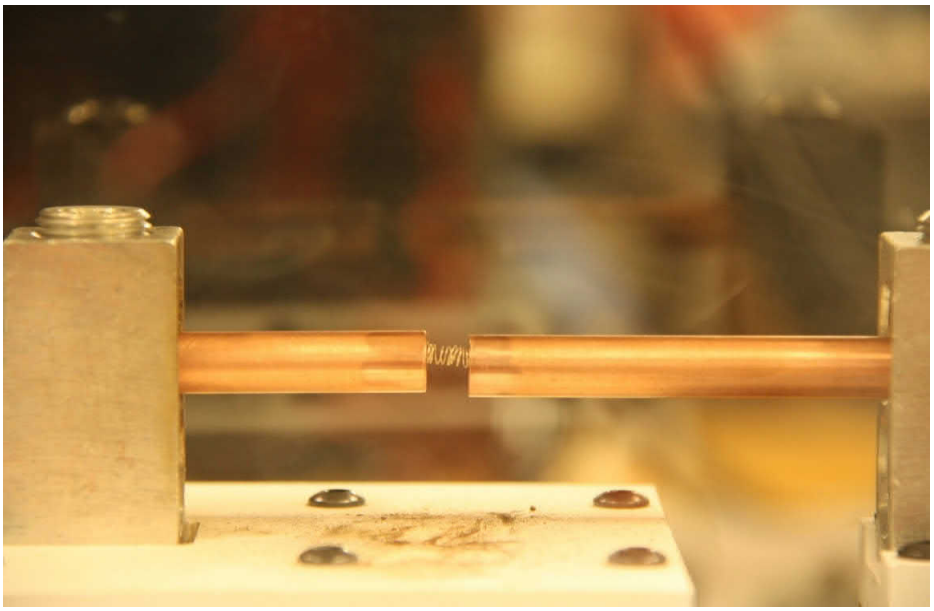

Fig. 5.2: Springed wire — detail of the test setup

The Springed wire test setup is displayed in Figure 5.2. Because of the higher currents, electrodes with larger diameter were used. The electrodes were positioned to form a fixed gap by a step motor. Apart from that, the setup and the used equipment were the same as in the case of UL 1699B tests, the gaps used for the testing were also the same as defined in the UL 1699B standard. Current levels measured were 50 A, 100 A and 200 A.

5.1.3 Power supplies used in the DC tests

The description of the DC test setup has to be complemented with a brief description of the power supplies used during the tests. While the PV panels were a good source of a noise-free DC power, due to the unpredictable performance of the roof-mounted PV panels (the power output was weather–dependent) and due to the fact that the overall power output was limited by the number of panels available, the Sorensen

DC power supply was used for the testing as well. Moreover, for the testing at 200 A (700 V DC) a custom-built DC power supply with 18-pulse rectifier was used.

5.2 AC Testing

The intended application field for the AC arcing detection is the AFDD as described in the standards. The measurements were done according to the standards. The data were collected for both the 50 Hz and the 60 Hz frequencies. For the 60 Hz the US grid was used as a power source, for the 50 Hz measurements the EU grid was used as a source.

The 60 Hz tests performed were the following:

1. Carbonated path tests,
2. Point contact arc test,
3. Unwanted tripping tests for:
    - Inrush current,
    - Normal operation,
    - Non-sinusoidal waveform,
    - Multiple loads and
    - Incandescent lamp burnout.

All loads prescribed in the standard were used for Unwanted tripping tests.

The 50 Hz tests done were:

1. Masking tests with all kinds of prescribed loads and
2. Series Arc Fault Tests.

Series arc fault tests were done using the Carbonated path test and Point contact test.

6 SIGNAL ANALYSIS OF THE DATA

6.1 The time domain

The data acquired during the arcing experiments were obtained in the time domain. The continuous analog quantities (currents and voltages) were then acquired using digital equipment (i.e., sampled with a given sampling frequency); thus, the input data for further analysis are discrete-time signals. Signal processing in the time domain is the first step in our effort to analyze how an arcing event influences the quantities of interest. In order to define methods for the detection of arcing events, it is necessary to understand the signals prior to the arcing event, during the arc ignition, and after the arc has been ignited. In this chapter, the signals will be shown in related figures, where the horizontal axis (x-axis) represents the time and the vertical axis (y-axis) stands for the signal magnitude. The graphical representation of the acquired data helps us to observe the overall signal magnitude, significant peaks, and typical patterns. In the last part of this chapter, the observations will be summarized in an attempt to define a typical arcing signature.

During the tests, the following signals were acquired:

- line voltage;
- arc voltage;
- unfiltered arc current;
- high-pass filtered arc current (cutoff frequency 10 kHz).

All of these signals were captured at the sampling rate of 5 MSPS (Million Samples Per Second), and therefore our captured signal data contain frequencies of up to 2.5 MHz.

As the 60 Hz and 50 Hz signals have the same characteristics, only the 60 Hz and DC data are to be introduced in this section.

6.1.1 Carbonized path test results: 60 Hz AC

The first presented signal data were acquired during a 60 Hz carbonized path test. The power source was an AC electrical grid with the frequency of 60 Hz; the arcing started at the time $t = 0.2\ s$.

As the circuit is fed from the grid, Fig. 6.1 does not show any changes in the supply voltage signal due to the low impedance of the voltage source. Although some high- frequency noise may be present in the line voltage signal as the arc voltage bumps periodically, as shown in Fig. 6.2,no changes to the line voltage are visible in the time domain.

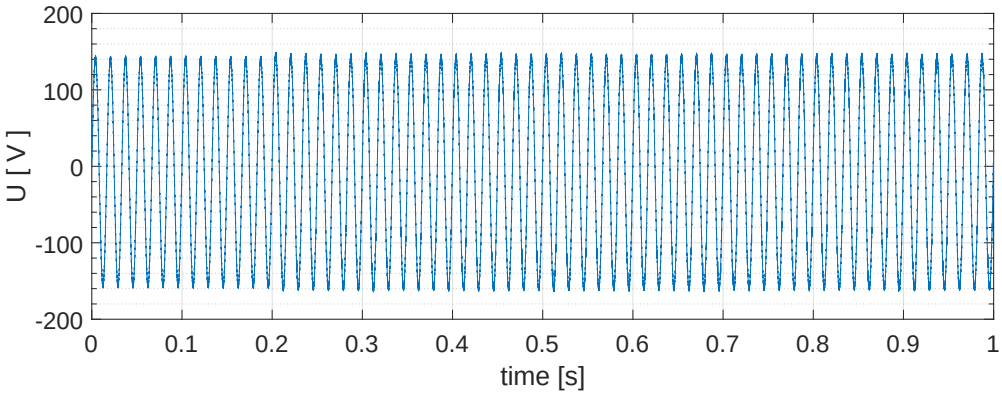

Fig. 6.1: The line voltage.

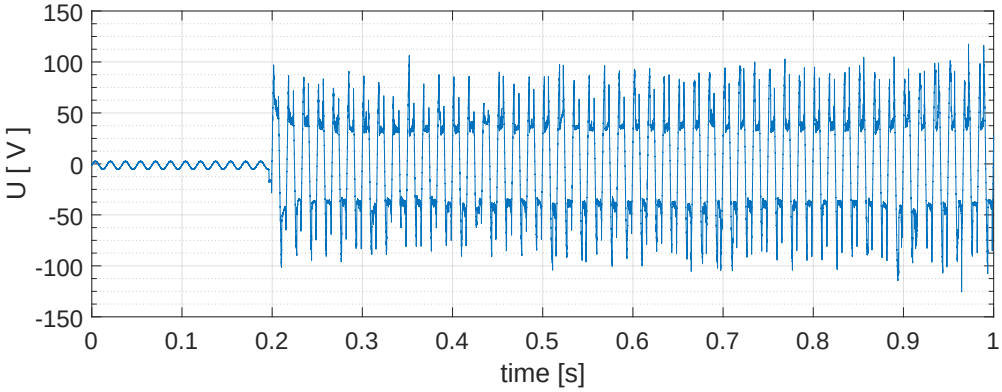

Fig. 6.2: The arc voltage

Before the arcing started, the arc voltage had been only a small, sine-wave shaped voltage signal caused by an alternating current flowing through the constant impedance of the test conductor. Once the arcing began, distinctive deviations from the smooth sine wave shape of the line voltage came to be present. The center part of each voltage half-period is flat; this flat part corresponds to the time period when the arc current has a non-zero value as the arc is established. The reason for the deviation from the sinusoidal shape of the signal is simple: When the voltage rises beyond a certain level, the arc ignites, the load is connected to the circuit, and the currents starts to flow. After the arc has ignited, the voltage across the arc drops, and the flat part of the signal indicates that the voltage drop across the arc remains almost constant as long as the arc remains ignited. At both the beginning and the end of the flat parts of the arc voltage signal, we can observe short transient events. Due to the possibly low impedance of the power source and the resulting low arcing signature in the line voltage signals, it is advisable to focus on signals related to the current flowing through the circuit (and through the arc).

In Fig. 6.3, the current of 22.5 A through the resistive load was measured as the signal of interest.

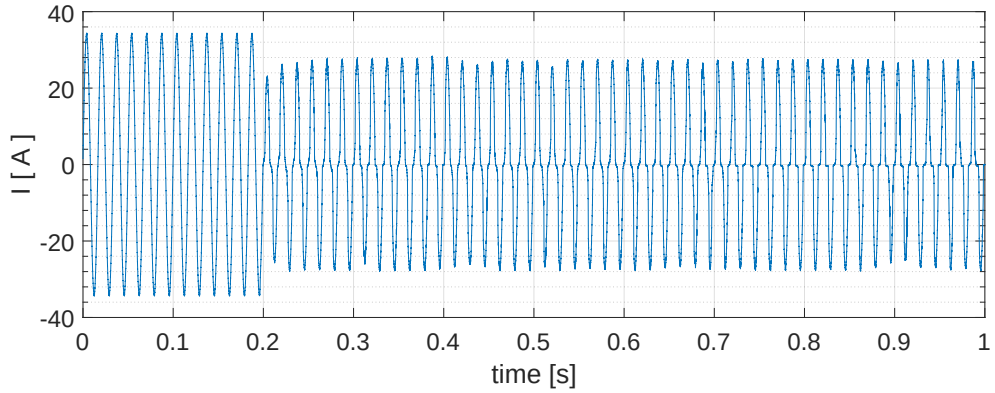

Fig. 6.3: The arc current

The acquired current signal is a regular smooth sine curve until the arcing starts at 0.2 s. Once the arc has ignited, we can observe the most significant feature of the AC arc current: the arc extinguishes itself when the voltage drops below a certain level, and if it rises again above the air-gap breakdown voltage, the arc re-ignites. The result of this effect in the time domain consists in short, nearly flat parts at the beginnings and endings of each half-cycle of the current signal.

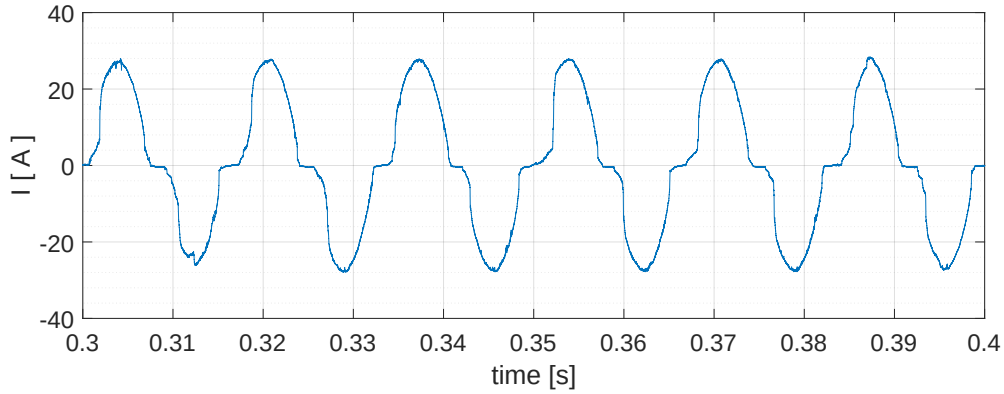

Fig. 6.4: The arc current — a detail.

If we look at the details of the current signal in Fig. 6.4, we can also observe a transient period at the beginning of the observed arcing event. We can see that, especially during the first few half-cycles after the arcing event started, the signal shape is highly irregular and the irregularities and short transients are quite random. Later we will see that randomness is the main feature of the arcing signal.

The last signal to be shown here is another current signal. This time, however, the signal data were filtered through a 10 kHz high-pass filter in order to eliminate

the low frequency components of the signal. Thus, in the signal data, only the frequency range between 10 kHz and 2.5 MHz remained.

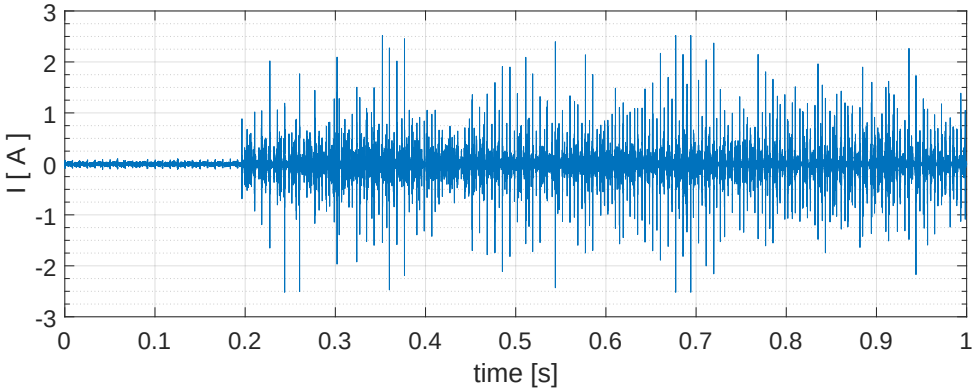

Fig. 6.5: The high-pass filtered arc current.

The filtered current shown in Fig. 6.5 5 is very different from the other signals, namely those we showed before. After filtering out the low frequency part, where the 60 Hz component dominated, the primary sine wave disappears. Instead, we observe multiple random bursts in the current signal, and these bursts are caused by the transient events observed at the unfiltered current signal. Such random-looking high frequency bursts are related to the flat parts, short transients, and random spikes observed in the unfiltered current signal data. More details on the randomness and irregularities are provided in Fig. 6.6 below, which indicates the beginning of the arcing event shown above.

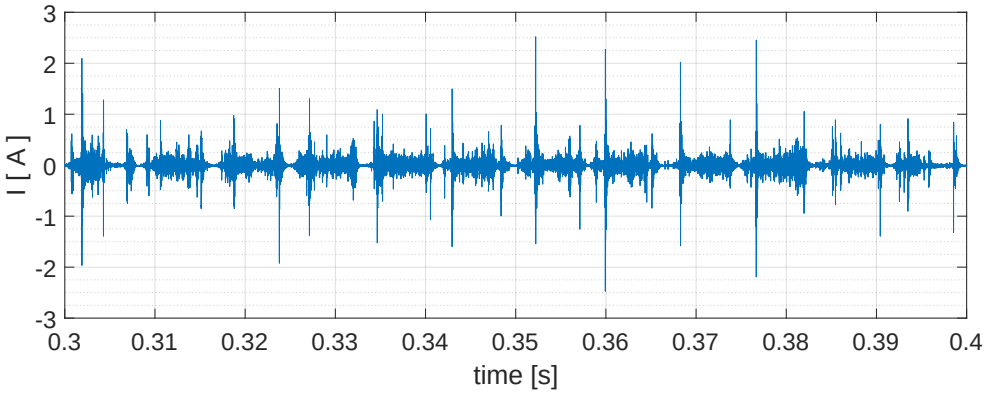

Fig. 6.6: The high-pass filtered arc current — a detail.

6.1.2 Opposing electrodes test: 60 Hz AC

The second set of data is also for 60 Hz arcing, but this time the arc was generated with the opposing electrodes test. The arcing starts at the time $t = 0.2\ s$; in this testing procedure, the electrodes were slowly drawn apart. The line voltage is again a smooth sine wave as shown in Fig. 6.1, and therefore we will not display it here.

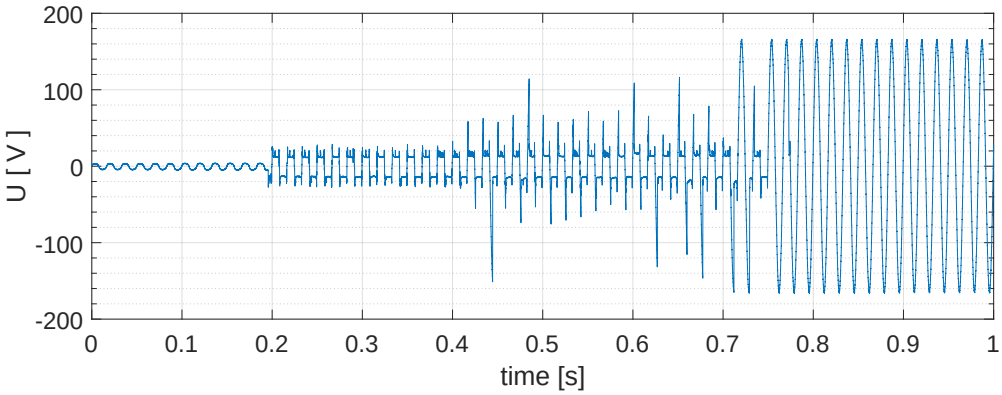

Fig. 6.7: The arc voltage.

The arc voltage shown in Fig. 6.7 resembles that of the previous event, but as the electrodes are slowly drawn apart, the length of the arc rises and so does the voltage across the arc until the arc is extinguished, the currents stops flowing, and the arc voltage becomes the smooth sine curve of the full line voltage. This test is applicable for describing and analyzing the arc behavior with various gap lengths.

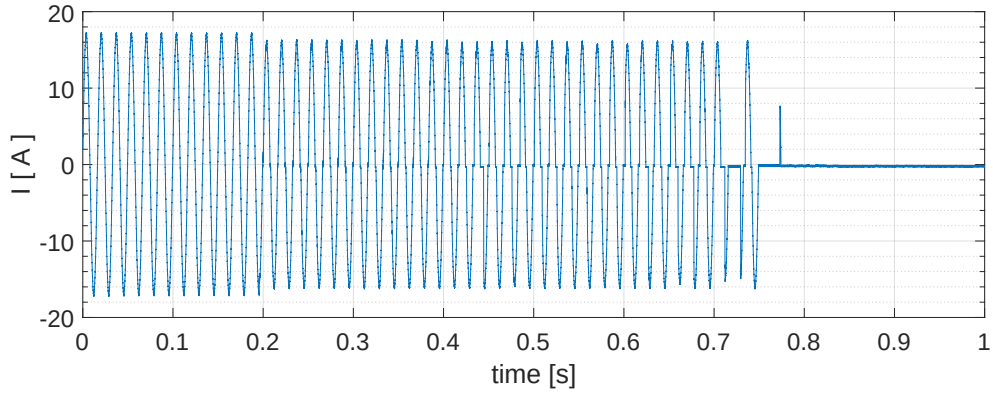

Fig. 6.8: The arc current.

The unfiltered current does not change much when the length of the gap is small. As the electrodes are drawn further away, we can observe increasing distortion of the current signal, and even one half-cycle of the zero current before the arc is fully

extinguished. Figure 6.9 indicates that the flat parts are very short and that many small random spikes are present in the primary sine wave.

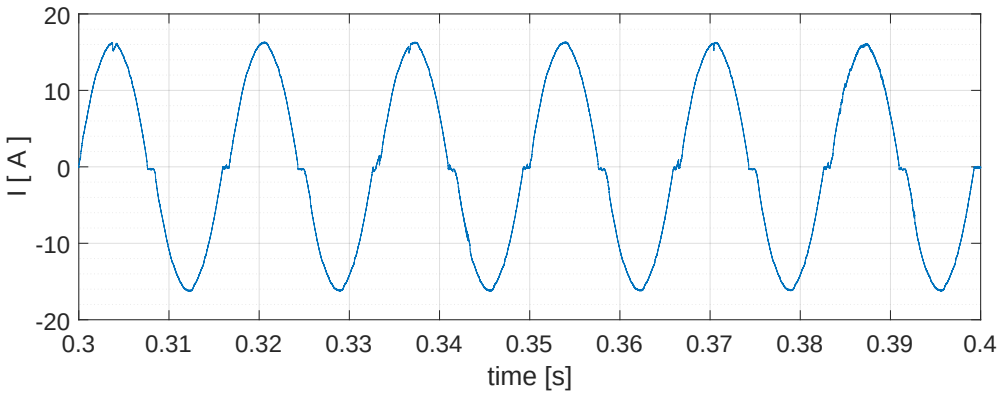

Fig. 6.9: The arc current — a detail.

In order to document the high frequency components that deform the primary sine wave shape, the 10 kHz high-pass filtered current signal data are shown in Fig. 6.10.

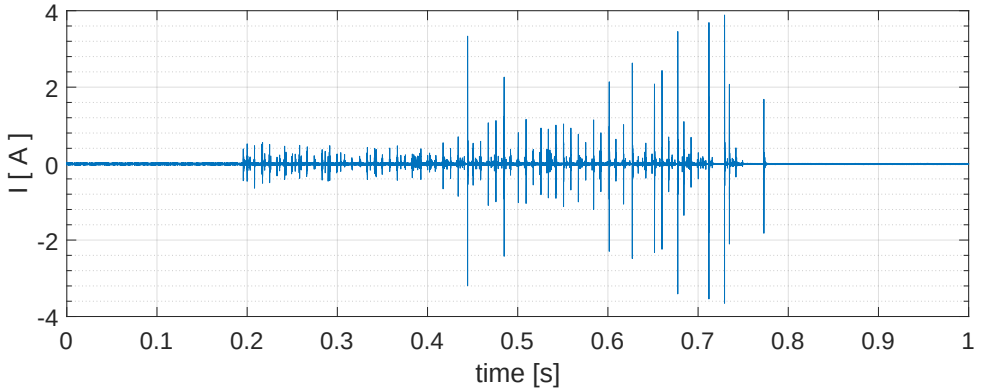

Fig. 6.10: The high-pass filtered arc current.

As long as the gap between the electrodes is small, we observe very little activity in the filtered data. Even when the gap rises and more spikes occur, the high frequency component remains relatively still and steady, which is in contrast with the results observed in the previous test. In this test, when some spikes are seen, they have highly variable peak values and occur randomly.

6.1.3 Point contact test results: 60 Hz AC

The third test is the point contact test as the point contact embodies the third way to ignite the arc according the standard UL 1699; this is a test that imitates

arcing as a result of an abrupt cutting of the cord. The fault current level of 300 A was used, and the cutting event occurred at the time $t = 0.2\ s$. This test usually does not produce long-lasting arcing, because the blade initially establishes a solid contact with one wire, and then, while the cutting movement continues, the blade makes a point contact with the other wire. Subsequently, as the blade cutting move continues, the blade makes a solid contact with that other wire, and a solid short circuit is formed. Short bursts of arcing are produced when there is a solid contact with the first wire and only a point contact with the other one. After a blade-caused short circuit has been fully established, there is very little or no arcing at all — depending on the size of the gap between the wires and the blade. The other current levels tested were 75 A, 100 A, 150 A, 300 A, and 500 A; as all of these exhibited similar characteristics, only the 200 A test results are shown.

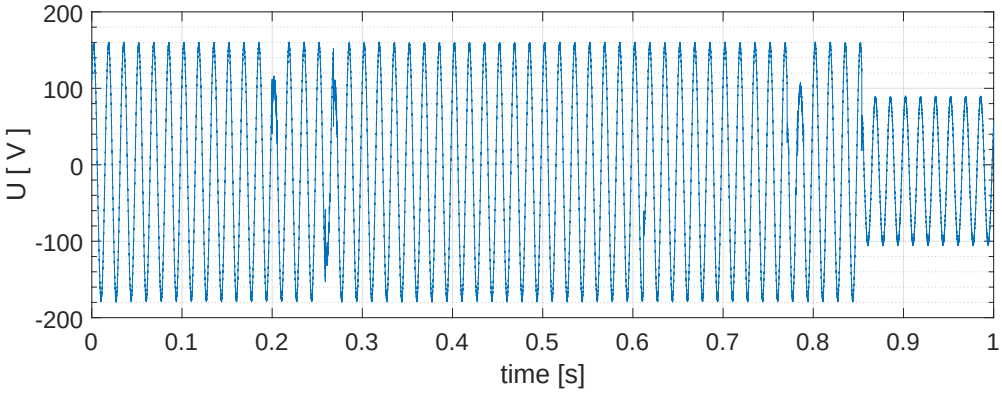

Fig. 6.11: The line voltage.

Due to the high current and the very fast and violent character of the cord cutting, we can observe changes in the line voltage as well. The arcing bursts that occur when the voltage of the arc changes will rapidly misshape the line voltage.

The arc voltage copies the line voltage, with the changes being more visible as the arc voltage is measured near the place where the blade cut was performed. When the half cycle of arcing is present, we can observe the flat centers of the arc voltage.

In the unfiltered current signal data (shown in Figure 6.13), we can observe random bursts of arcing. There are several bursts with the current signal deformed so much it almost does not resemble the original sinusoid shape. When the arcing stops, the blade-caused short circuit is formed, and the circuit starts to conduct. However, the shape of the current signal exhibits deformation similar to that shown when the arcing was present; such deformation is represented in Fig. 6.14.

In the 10 kHz high-pass filtered signal, we can observe several bursts caused by the arcing. These bursts occur at random times and are characterized by varying peak values.

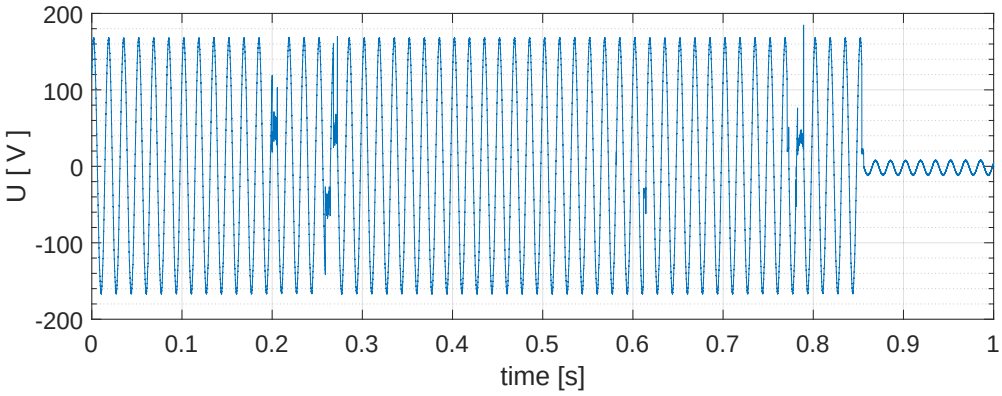

Fig. 6.12: The arc voltage.

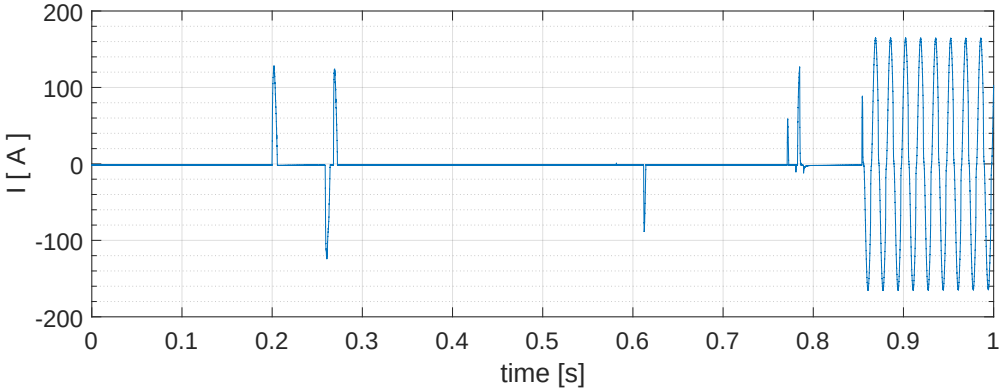

Fig. 6.13: The arc current.

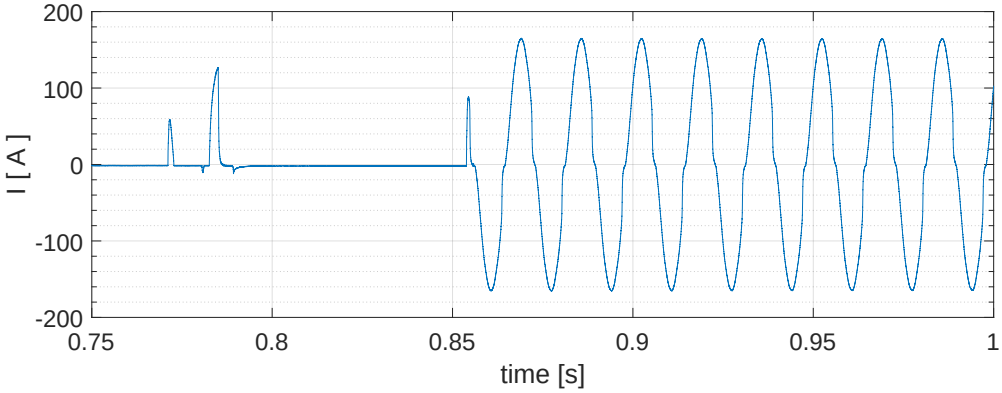

Fig. 6.14: An arc current detail.

6.1.4 DC tests

In the following section, we will concentrate on DC arc signal characteristics in the time domain. The most important difference is the nonexistence of a zero crossing

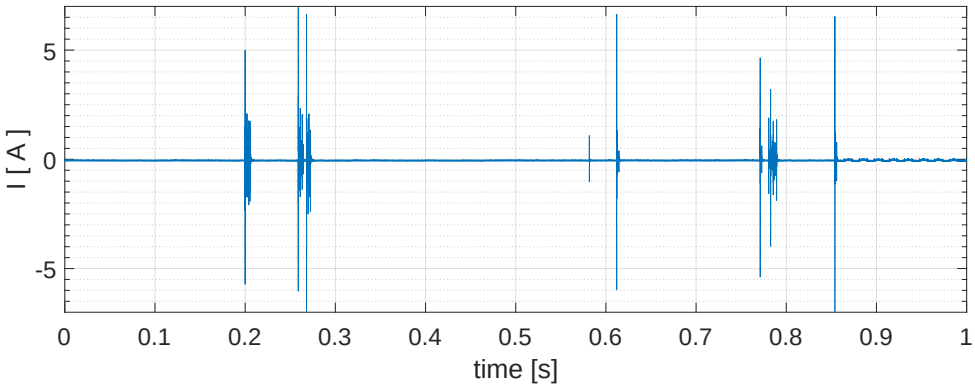

Fig. 6.15: The high-pass filtered arc current.

region for the DC supply voltage; thus, repeated arc ignitions do not occur. Althogh the reason is clear, the nonexistence of repeated transients (repeated arc ignitions) makes finding the signature of the DC arcing a highly challenging task. In spite of the fact that tests were performed for both low currents (using the procedure described in the UL 1699B standard) and high currents, only tests with the higher ones (more than 40 A of arc current) will be presented here. The reason is simple: After evaluating the results of all the tests performed, we found out that the high current tests provide results different from those obtained with the low current tests. In both cases, the DC arcing signal is obviously assumed; as regards the low currents, however, the arc is less stable and thus also more "violent". In the low current signal characteristics, we may observe many transient events and much higher high-frequency noise than in the high current signals. For the intended application, it is necessary to focus the analytical effort on the more challenging high-current data.

The DC arcing tests were performed with two different power sources, one of which is a PV power plant with no converter installed. From this source, the feeding current is extremely stable, with almost no noise, as displayed in Fig. 6.16. The high frequency (10 kHz to 2.5 MHz) current is less than 1 A, while the overall current corresponds to 67 A.

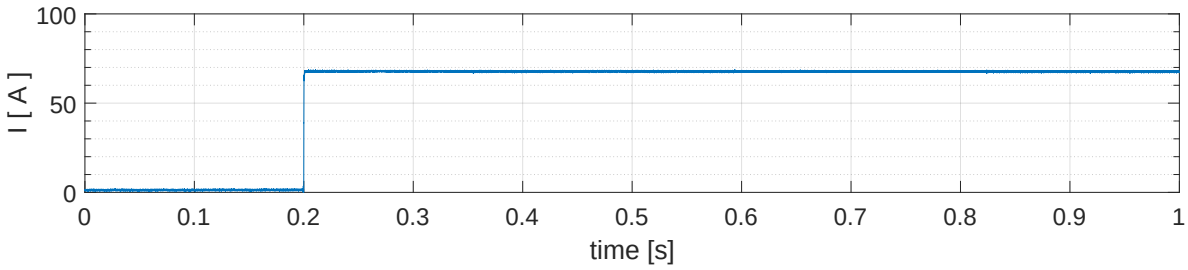

Fig. 6.16: The PV power supply: DC current — a baseline test.

The other source of the DC electric power is a custom DC power supply. As shown in Fig. 6.17, this power supply exhibits many little peaks in a non-filtered current signal. If we zoomed in, we would observe that these peaks are periodical. However, as for the high frequency signal, it is nearly same as in the case of a PV source.

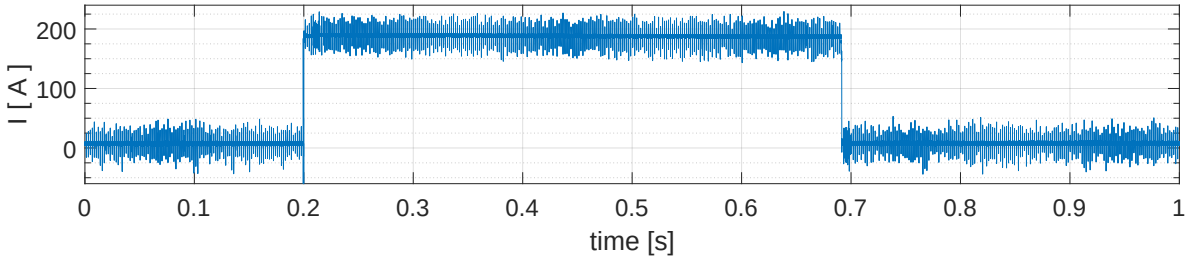

Fig. 6.17: The DC power supply: DC current — a baseline test.

In the DC tests, two different arc initiation procedures were used; while the former one is a classic steel wool and plastic tube arc generator as described in the UL 1699 standard, the latter one consists in a springed wire test setup. These methods were already described in chapter 5, and thus we will not analyse them again at this point.

The first test characterized here is that with PV panels as the power source, where the arc is ignited with steel wool held in place by a plastic tube. The line voltage is 295 V, and the pre-arc current corresponds to 72 A; the current drops to 61 A during the arcing event. The arcing starts at the time $t = 0.2\ s$.

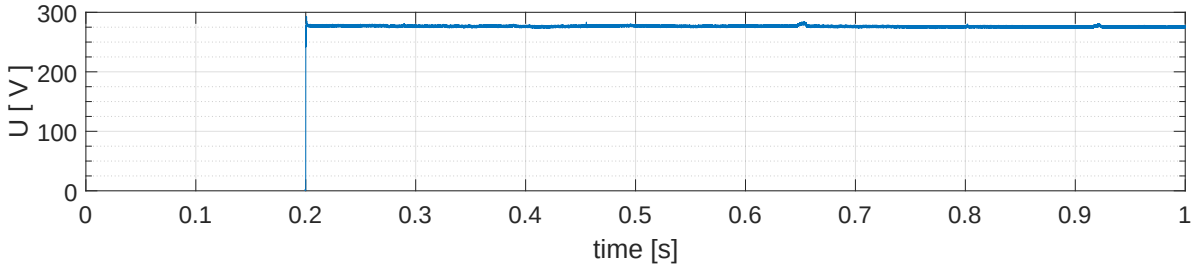

Fig. 6.18: The PV power supply: Line voltage during test.

When we observe the line voltage, it seems at first that there is not much to be seen. The voltage looks smooth, with no possibility of finding out whether arcing present in the circuit.

However, if we examine in detail the spot where the arc ignition was expected to occur, we will observe a transient event with the duration of approximately 1 ms. The voltage quickly rises to 290 V, and this rise is accompanied by many small spikes and rapid variations of the voltage.

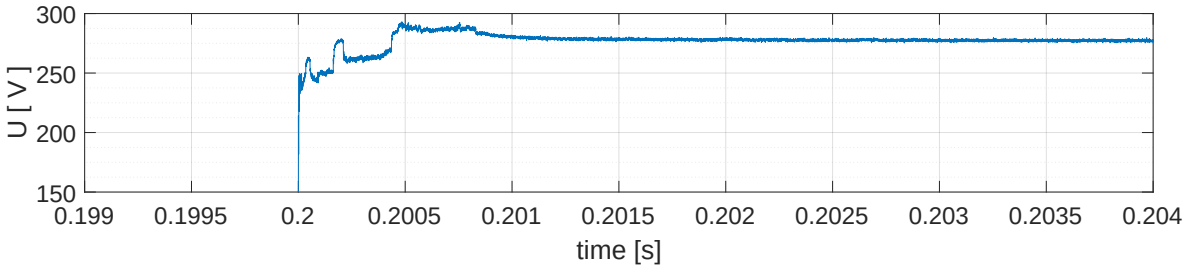

Fig. 6.19: The PV power supply: The line voltage during the arcing test — a detail.

When observing the unfiltered current signal, we can notice it is more eventful than the voltage one. Because the arc is not static every time its root changes its position, the arc impedance varies, and we may observe a fast small drop or rise in the current value.

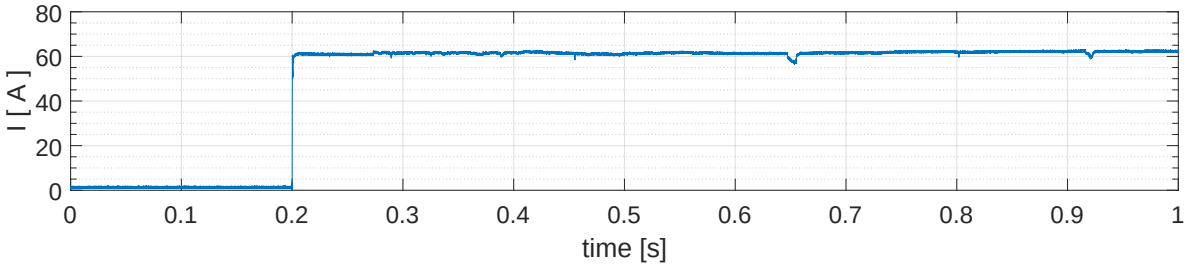

Fig. 6.20: The PV power supply: the current during the arcing test.

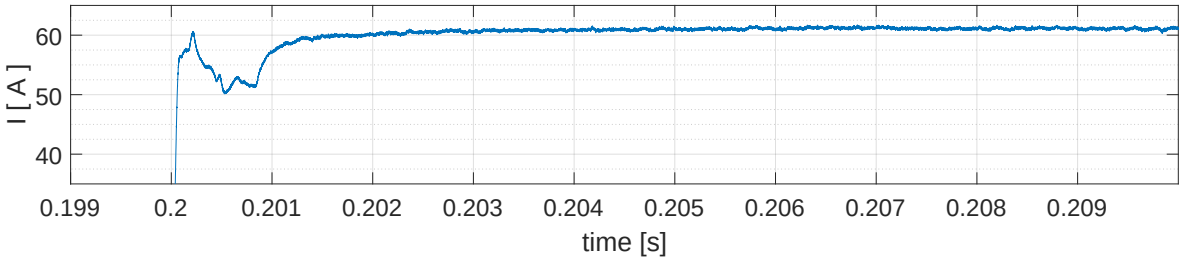

Fig. 6.21: The PV power supply: Current during the arcing test — a detail.

The detail of the current signal shows the transient event when the power is being switched on. The current drops down to the value of 50 A, and the whole event lasts for approximately 3 ms. We can also observe some of the small transient events related to the unstable nature of the arcing process.

The 10 kHz high-pass filtered current signal is shown in Fig. 6.22, where most significant event is the first (and the highest) peak; additionally, there are some subsequent transient events while the arc is burning. The mean value of the high frequency signal is 0.065 A.

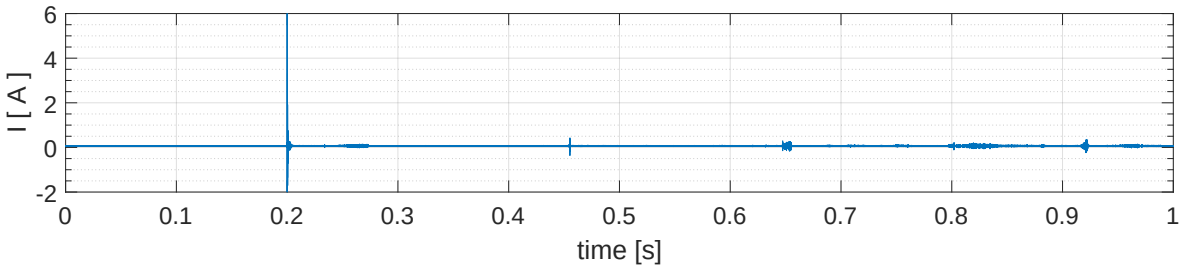

Fig. 6.22: The PV power supply: The high-pass filtered current.

6.1.5 Novel arc ignition procedure

In the previous examples, the arc signature could not be described due to our inability to separate the transients related to the closing of the circuit from those associated with the initial ignition of the arc. This obstacle is solved by a newly proposed arc ignition procedure (the springed wire test); the last two examples in this chapter describe various tests using this novel approach.

The first test uses PV panels as the DC voltage source. In this case, the unfiltered arc current will be displayed first in order to show when exactly the arcing started. With this additional information, we will observe the other signals.

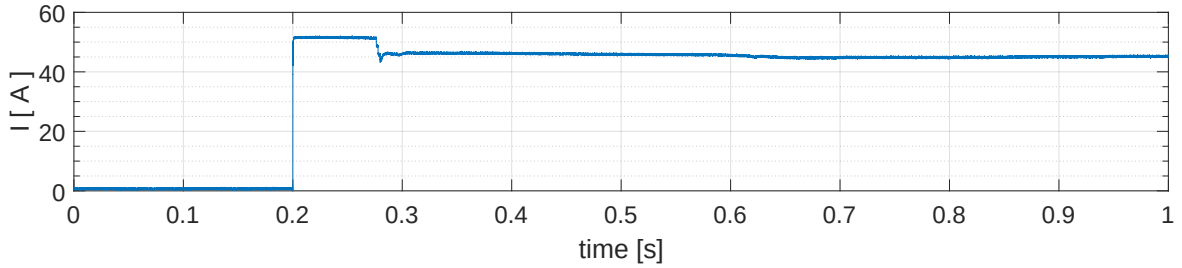

Fig. 6.23: The PV power supply: The current during the springed wire test.

As indicated in Fig. 6.23, the circuit was switched on at the time $t = 0.2\ s$ with the current value of 48.6 A. The arcing began later, at $t = 0.27\ s$. The arc ignition is accompanied by a transient event of the current dropping down to the value of 41.6 A before it settles at the stable value of 43.5 A. The transient event lasts for approximately approximately 10 ms.

It is obvious from the line voltage representation (Fig. 6.24)that there is nothing to observe at the time of the arc ignition, and thus we can state that the arcing with the current value of (roughly) 50 A does not influence the source voltage signal. Theoretically, if the source had a higher impedance, the line voltage could change.

If we look at the 10 kHz high-pass filtered current signal, we can observe that both the closing of the circuit and the beginning of the arcing are visible events. To improve the visual resolution, it is advantageous to transform the data so that the

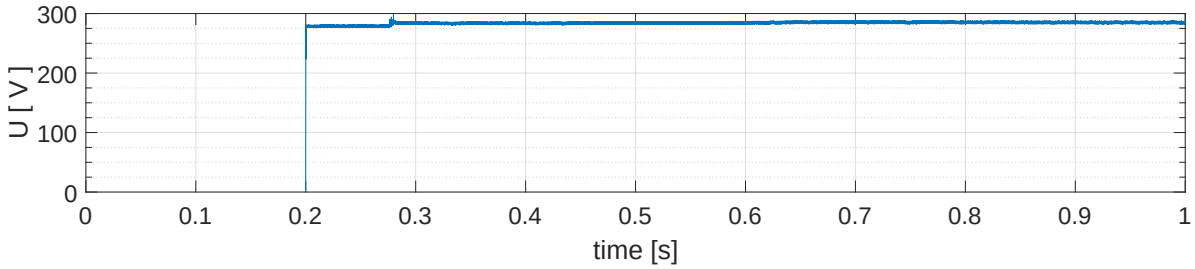

Fig. 6.24: The PV power supply: The line voltage during the springed wire test.

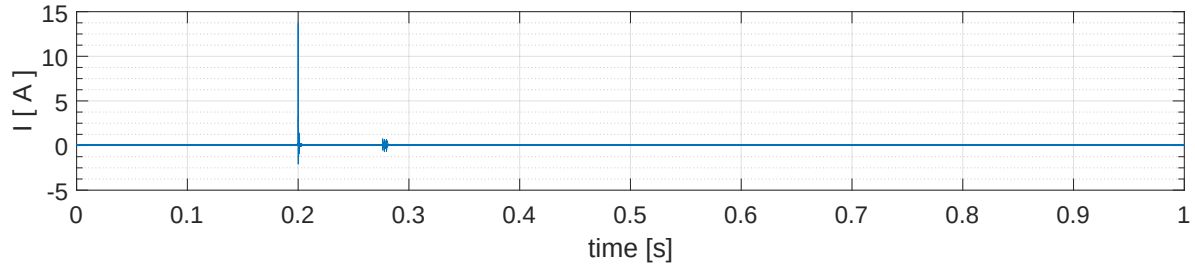

Fig. 6.25: The PV power supply: The high-pass filtered current — the springed wire test.

current axis (y-axis) can be changed to a logarithmic scale (dB scale). The result of such a step is shown in Fig. 6.26.

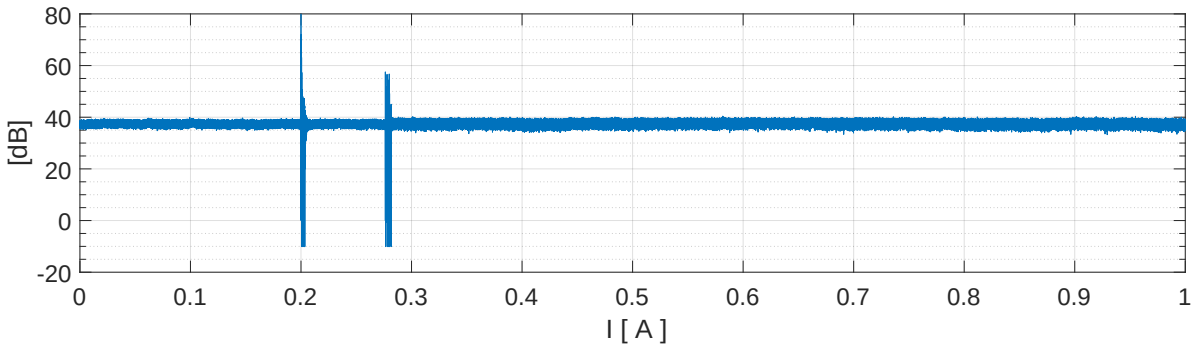

Fig. 6.26: The PV power supply: The high-pass filtered current, a dB scale.

The modified resolution is substantially better, and, in addition to the clear demonstration of both main events, it is possible to observe that the signal width becomes visually thicker once the arc has been established; in other words, once the arc is ignited, the amount of high frequency noise is elevated.

The last data presented in this chapter were acquired with a custom built DC source as the power source; its voltage was 680 V, and the current corresponded to 200 A. The voltage and current levels were much higher than in the previous cases, and they remained in the range of the current levels of the intended applications.

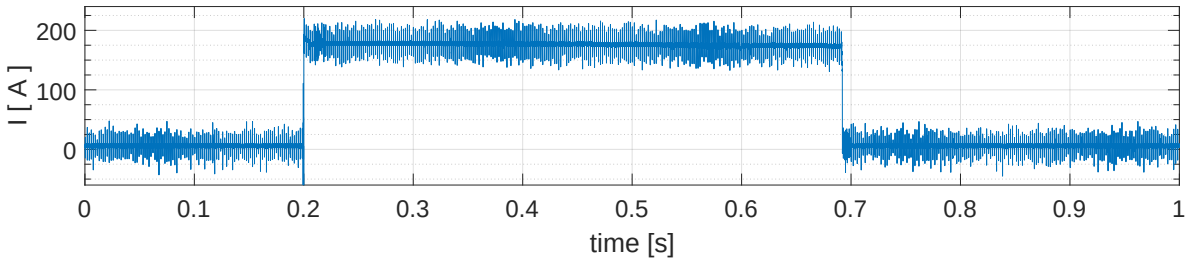

Fig. 6.27: The DC power supply: The current during the arcing test.

At the first stage, the unfiltered current signal will be presented in order to provide a good overview of the whole test. Because of the very high current, the arc ignites almost immediately after the circuit is energized; however, we can still recognize when the arcing started. The main distinguishing feature of this signal is the periodical peaks, which, in the figure above, resemble a light blue envelope around the main dark blue signal. These light blue peaks are generated by the power supply and do not bear any relevance to the arcing. We will be able to observe them in the 10 kHz high-pass filtered current signal as well.

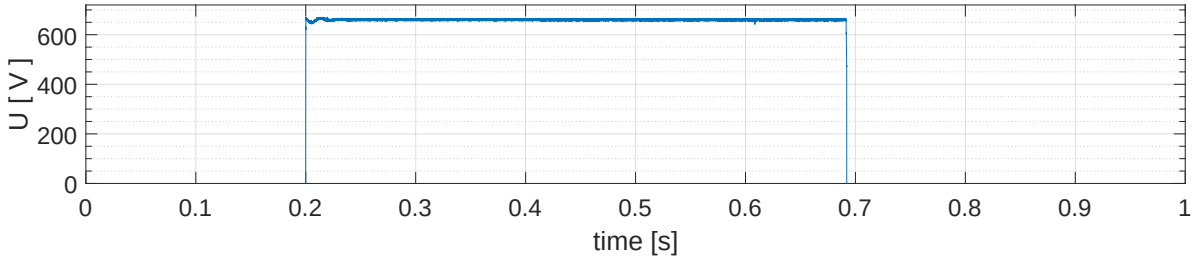

Fig. 6.28: The DC power supply: The voltage during the arcing test.

The line voltage signal represented in Fig. 6.28 shows the transient event at the energizing circuit and the immediate arc ignition, but apart from these not much is to be seen. In Fig. 6.29, the 10 kHz high-pass filtered current in the absolute scale is displayed.

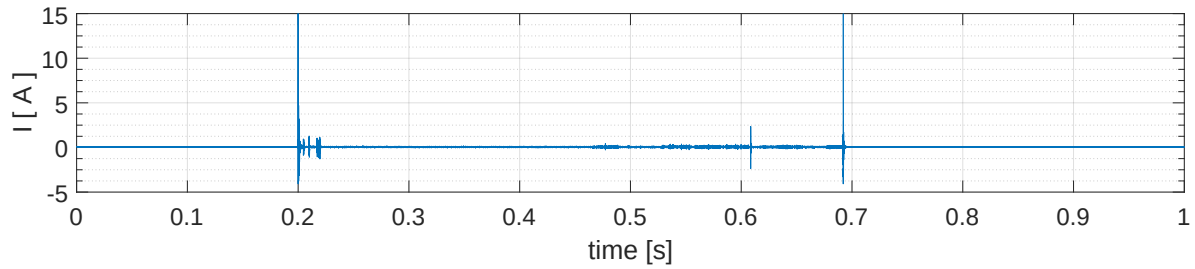

Fig. 6.29: The DC power supply: The high-pass filtered current during the arcing test.

However, to gain more information from the high frequency current signal, signal transformation and conversion of the vertical axis to a dB scale are used again (see Fig. 6.30 for the result).

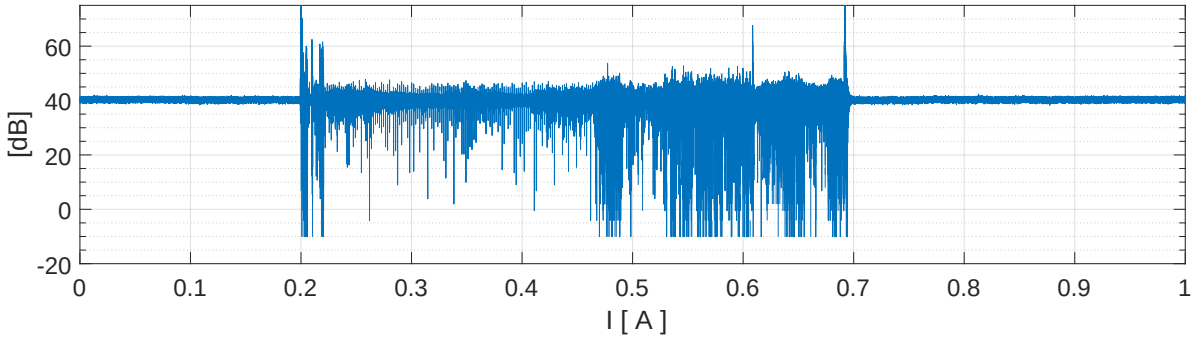

Fig. 6.30: The DC power supply: The current during the arcing test, a dB scale.

In both cases, it is obvious that arcing is present, but we are unable to find the exact moment of its beginning. Moreover, in both cases we can also observe periodical peaks generated by the power supply; these regular peaks are shown in detail in Fig. 6.31.

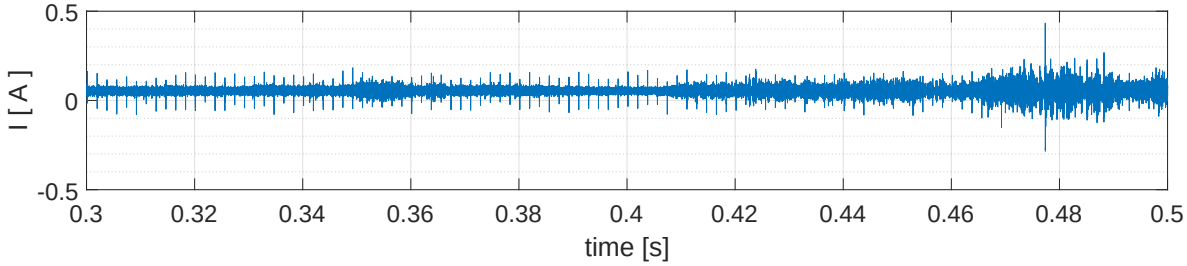

Fig. 6.31: DC power supply: High-pass filtered current — detail

6.2 The frequency domain

As stated in the previous chapter, we need to obtain more information from the acquired signal data to facilitate arcing detection. In order to make the additional information available, we will shift our signal processing domain from the time one to the frequency one. Thus, we will perform the Fourier transform (FT) of the time domain signal. This transform is essentially a convolution between the time series x(t), represented by samples x(k), and a series of sine and cosine functions that can be viewed as template functions. The operation measures the similarity between the x(t) or x(k) and the template sine/cosine functions, and it expresses the average frequency information during the entire period of the signal analyzed [13].

The obtained signal is discrete, meaning that the discrete Fourier transform (DFT) has to be used. The most efficient algorithm for the DFT is the fast Fourier transform (FFT); the FFT's speed stems from the fact that the original computational complexity of the signal N^2 is reduced to $N * log_2(N)$. Therefore, the demand for the computing power is much lower (for $N \geq 4$) [21].

The obvious drawback of using the FT lies in that the method does not provide any information about the evolution of the signal in time, as it ensures results in the frequency domain. Another disadvantage of the FT is the assumption that the input signal is periodic; however, any violation of this assumption leads to distortions that are still acceptable.

As we need to analyze signals having a non-stationary character (their frequency content changes in time), information on the evolution of the signal in time is crucial. This problem can be addressed via taking advantage of the concept presented by Denis Gabor in 1946; the solution is to divide the signal into small time windows, where we assume this signal to be stationary. Such division is achieved via multiplying the signal by a window function. For each windowed function, an FFT is then computed. Such representation of the frequency domain variations over time is referred to as the short-time Fourier transform (STFT).

The length of the window is important for the resolution of the time and the frequency. When we tile the time-frequency plain with the STFT, the area of one tile remains the same, although the length of the tile can be changed. This means that, with a long window, we obtain a higher resolution in the frequency domain but lose the resolution in the time domain. In an extreme case, the window length is the whole duration of the measurement the information is completely lost . In the opposite case, the window is narrow, and the resolution of the time content is high. But the gain in the time resolution was lost in the frequency resolution, and thus it is important to choose an appropriate length of the window function.

The plot used to visualize the STFT data is termed a *spectrogram*. The result-

ing 2D spectrogram shows the magnitude of the time-dependent Fourier transform versus time; the magnitude itself is represented by color changes. In the 3D spectrogram, the z-axis is present as well, and displayed in its direction is the magnitude of the signal.

While analyzing the acquired spectrograms, two significant patterns can be noticed. The former one is important as it helps us to better understand the signals acquired during the arcing, regardless of the fact that the observed phenomenon is not directly relevant for the arc detection. The phenomenon manifests itself as peaks and valleys created by standing waves. To explain this behavior, let us cite the definition of standing waves first:

> *"A standing wave is an oscillation pattern with a stationary outline that results from the superposition of two identical waves traveling in opposite directions."* [18]

And how is this definition related to our application? When the sine wave in the transmission line travels through the boundary where the impedance changes, a part of the wave moves forward, and another part is reflected in the opposite direction. This is the reason why there are waves propagating in two directions with the same frequency and amplitude in the electrical circuit. Because of the additive behavior of the waves, the amplitude of the resulting wave is different from the wave fed to the circuit from the source. The two most visible cases are when the amplitude doubles or is zero; these two cases are then denoted as peaks and nulls.

The standing waves are observable at high frequencies, namely when the length of the transmission lines is not negligible with respect to the length of the waves. In the spectrogram, we will observe them as peaks and valleys (bands of amplified and attenuated signal magnitudes) at a given frequency going through the whole time when the current is flowing through the circuit. For the arc detection, it is important to understand that arcing emits a substantial amount of high frequency noise to the electrical circuit, and therefore the chance of the peaks and valleys (nulls) occurring is very high. However, to use this phenomenon for arc detection is a problematic task as the differences in the wiring topology of every installation directly influence the positions and magnitudes of the peaks and valleys.

The latter observable phenomenon is the broadband noise bursts affecting the whole spectrum. In the 3D spectrogram, these will be displayed as thin walls throughout all the frequencies. The bursts are the sign of a fast step change in the current signal. Such changes are present when the circuit is energized and de-energized; when the arcing starts; and also randomly during the arcing event. The randomness in the description of the arc behavior is important as it is the randomness that helps us to distinguish between load-generated high frequency noise and

arc-generated high frequency noise.

The test measurements displayed here are the same as those characterized in the Time domain chapter. We will present 3D and 2D spectrograms of the 10 kHz high-pass filtered current (with one exception), and, for better understanding, also the relevant unfiltered current signal in the time domain.

6.2.1 Carbonated path test: 60 Hz AC

The first presented test is a 60 Hz carbonated path test. In this case, the 3D and 2D spectrograms of the unfiltered current signal are introduced first so that the reader understands why only the high frequency data are used in the remaining examples.

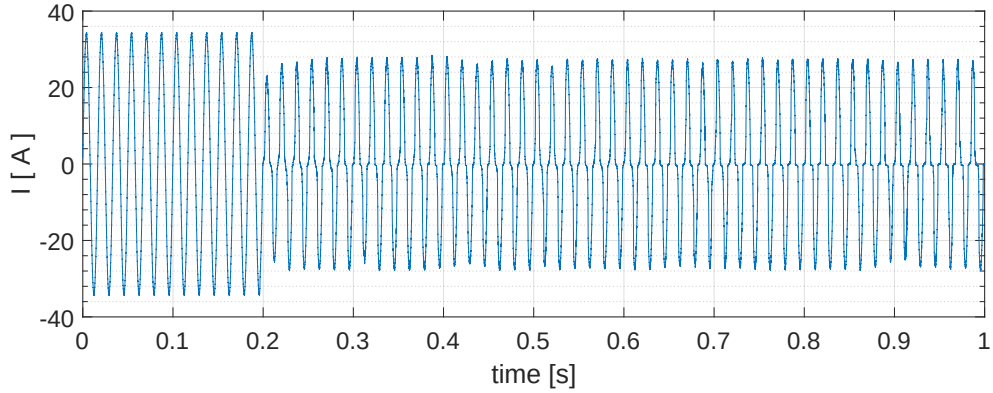

Fig. 6.32: Carbonated path test: Arc current

At the time $t = 0.2\ s$, the arcing has started. The arc ignition corresponds to a decrease in the flowing current as the arc represents an elevated impedance in the current path.

The 3D spectrogram has three axes: an x-axis displaying the frequency, a y-axis expressing the time, and a z-axis displaying the magnitude of the signal at the decibel scale. We can observe a very high signal magnitude in the region of low frequencies. Also, many broadband bursts are observable over all the spectrum width, forming the so-called walls are present. In this figure, we cannot see any peaks or nulls formed by the standing waves. The walls are visible in the following 2D spectrogram (Fig. 6.34) as vertical lines that correspond to elevated broadband magnitudes at given times.

The spectrograms below show the same test, but the input current signal for the STFT was a high-pass one filtered, with the cutoff frequency of 10 kHz. Due to the high pass filter, the strongest signal part up to 10 kHz was eliminated. However, it can be observed that the overall signal magnitude was lowered; it appears as if the whole base of the signal were missing. This, then, is the consequence of the

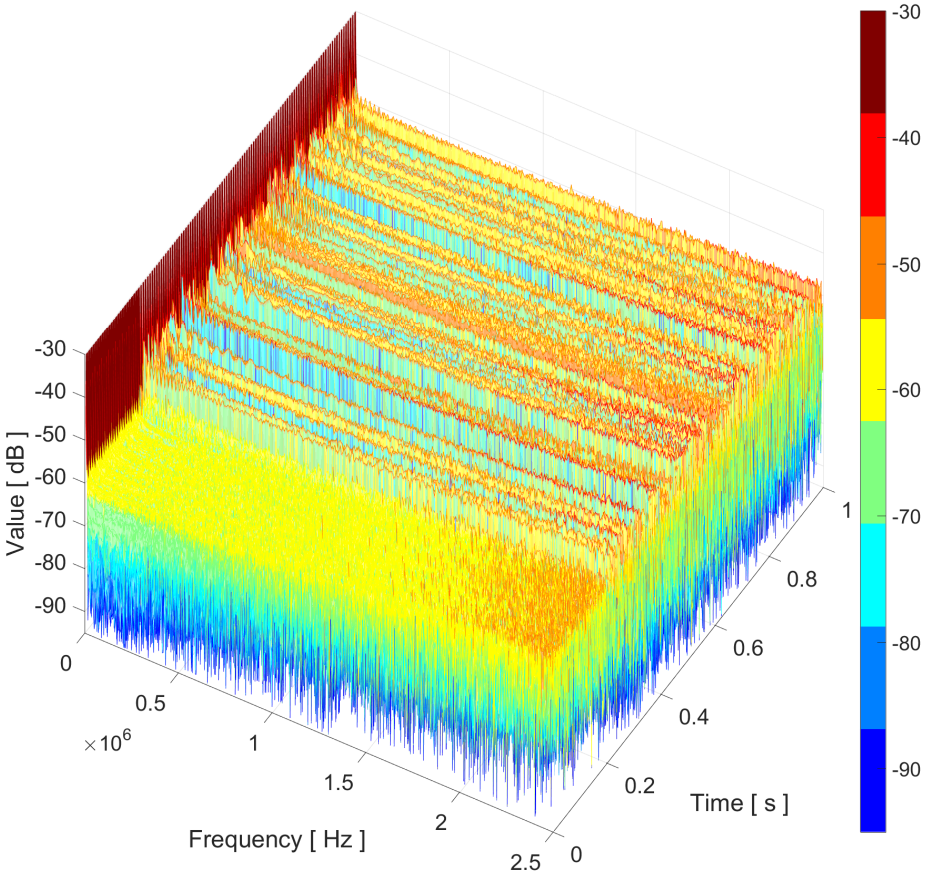

Fig. 6.33: The carbonated path test: The arc current — a 3D spectrogram.

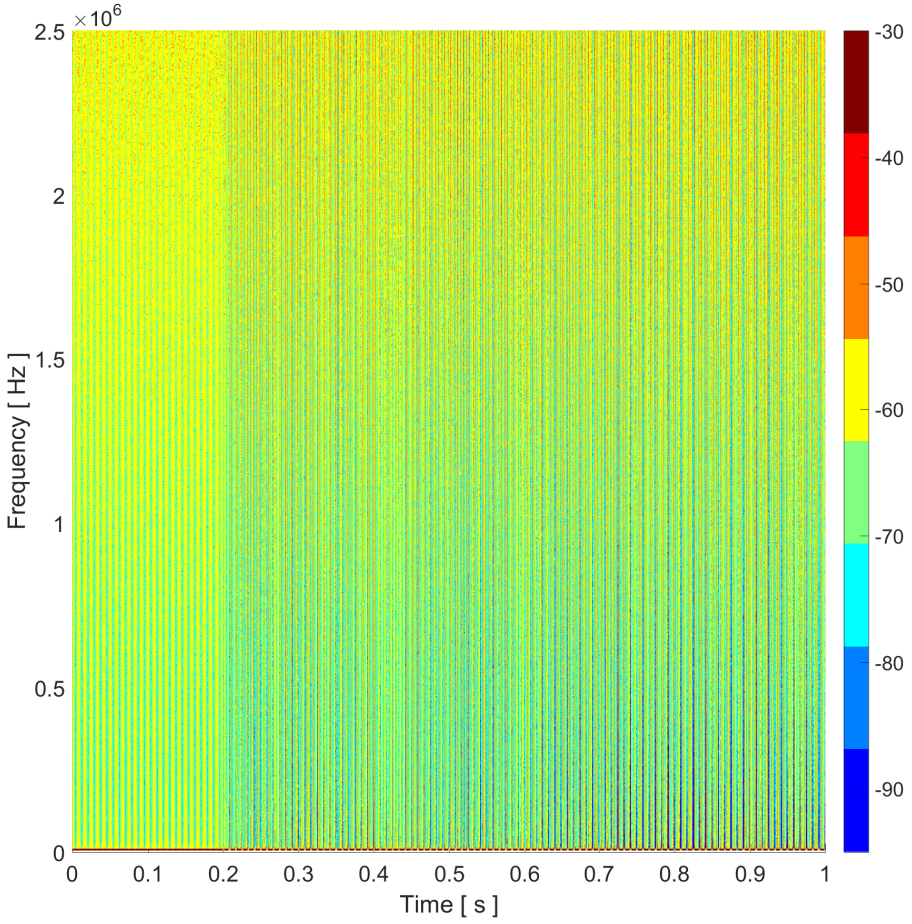

Fig. 6.34: The carbonated path test: The arc current — a 2D spectrogram.

windowing used in the STFT, aand the effect is referred to as frequency leakage. In this case, a strong low frequency component present in the input signal is leaking to the high frequency part of the spectrum.

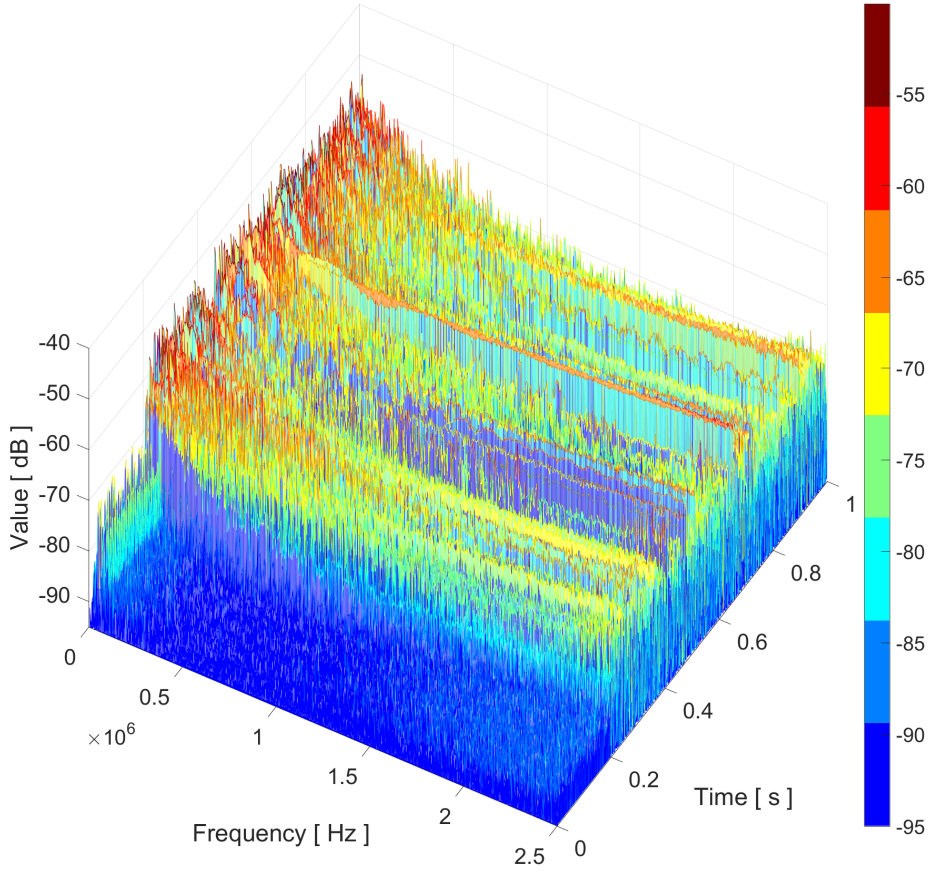

Fig. 6.35: The carbonated path test: The high-pass filtered arc current — a 3D spectrogram.

The origin of frequency (spectral) leakage can be explained as follows [8]:

> *"...the observed signal is actually convolution of 'ideal''(infinite, periodic) signal with a windowing function. The used window function (rectangular window) represents itself as a sinc function in the frequency domain and as such it has side lobes other than its main lobe. Those side lobes are not desired and they represent spectral leakage in frequency domain."*

Using a more advanced windowing function could help us to tackle the difficulty; however, the use of high-pass filtered data is a robust solution that completely removes the problem. The high-pass filter eliminated the strong low frequency (60 Hz) signal, and thus significantly less "energy" is available for the leakage,

making the high frequency part of the spectrogram much less distorted. In the STFT spectrogram of the 10 kHz high-pass filtered current signal, the broadband bursts affecting the overall spectrum are easier to recognize and detect.

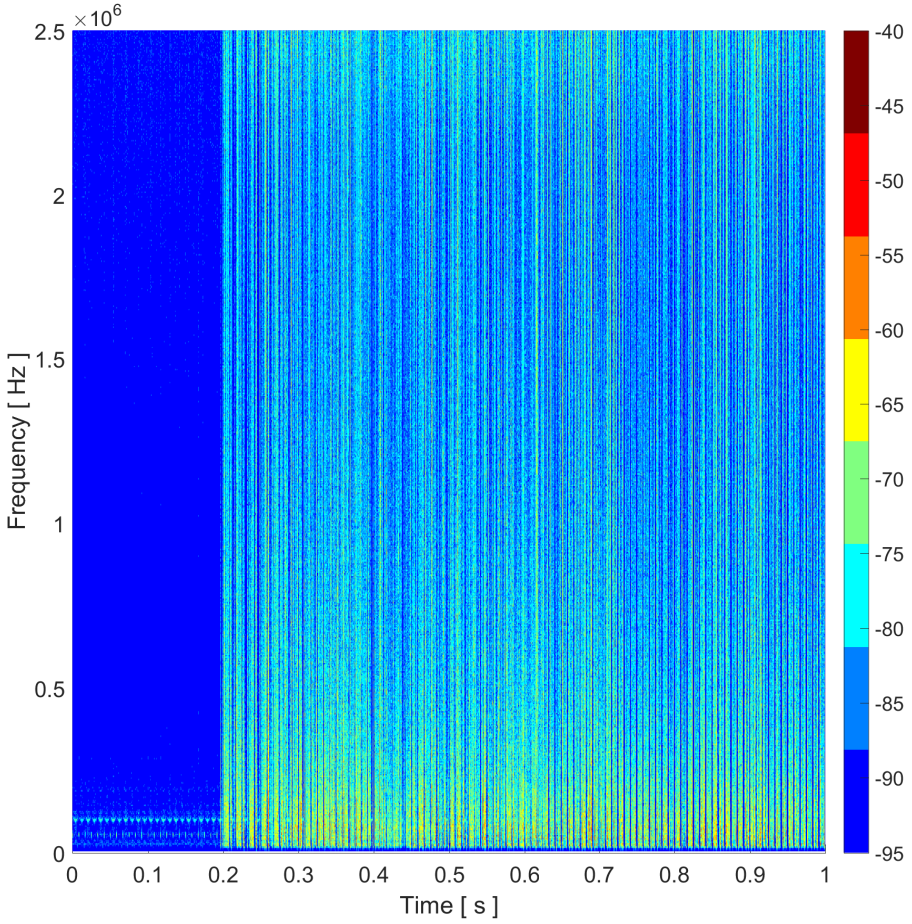

Fig. 6.36: The carbonated path test: The high-pass filtered arc current — 2D spectrogram.

6.2.2 Opposing electrodes test: 60 Hz AC

The second presented test is the 60 Hz opposing electrodes test, a procedure where the electrodes are slowly drawn apart.

The unfiltered time-domain current data are shown in Fig. 6.37. The arcing starts at $t - 0.2\ s$, and the small drop in the current is caused by a non-zero impedance of the arc. As the electrodes are slowly drawn apart, the length of the arc rises. Due to the increasing distance of the electrodes, the arc then starts to diminish at $t = 0.7\ s$.

In the corresponding spectrogram (Fig. 6.38) we can again observe broadband noise bursts at distinct times.

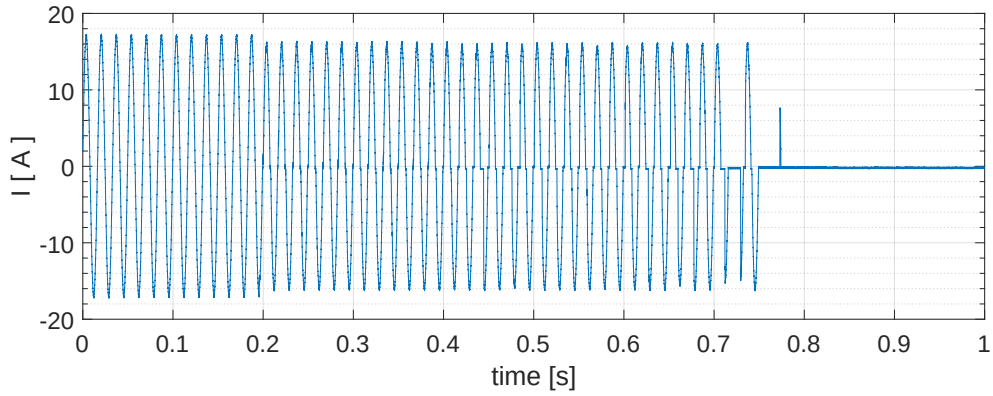

Fig. 6.37: The opposing electrodes test: The arc current.

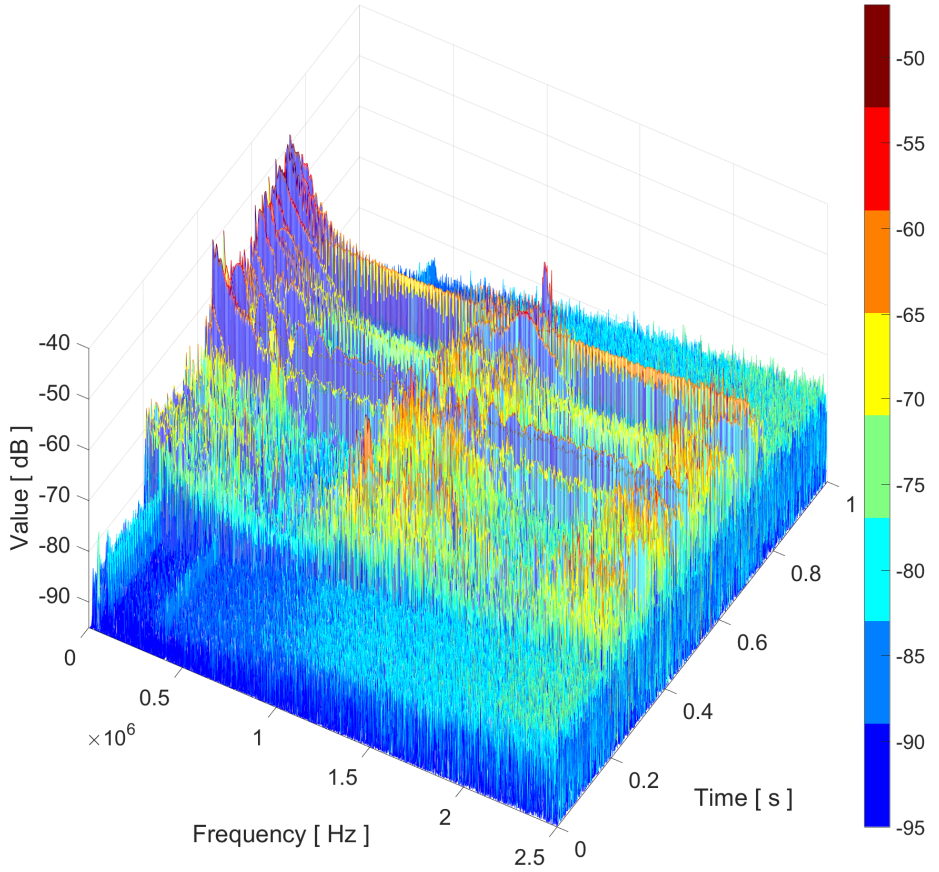

Fig. 6.38: The opposing electrodes test: The high-pass filtered current — a 3D spectrogram.

In this 3D spectrogram, the peaks and valleys caused by the standing waves are also observable in the form of long-term elevations at specific frequencies. The effect of the standing waves is more prominent in the 2D plot, where the standing waves

are highlighted as horizontal lines.

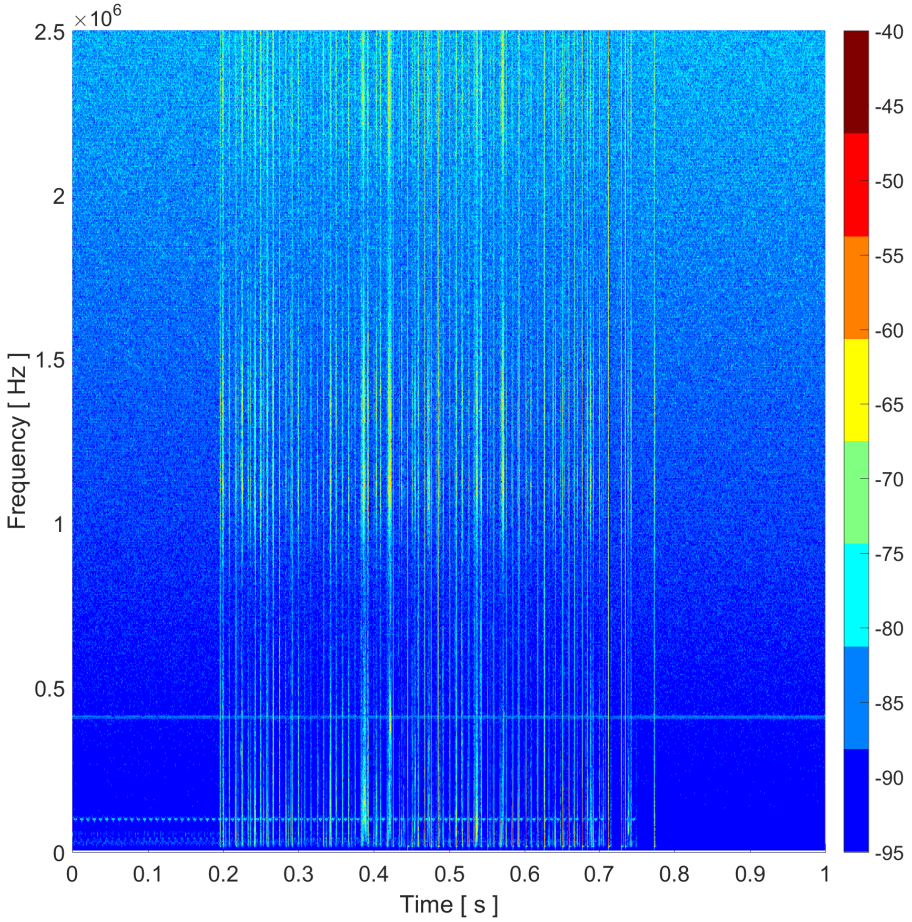

Fig. 6.39: The opposing electrodes test: The high-pass filtered current — a 2D spectrogram.

6.2.3 Point contact test: 60 Hz AC

The last 60 Hz test presented is the point contact test, namely a cutting procedure where a cable specimen insulation is cut with a suitable tool having a steel blade.

The arc current is present in the form of short bursts before the conductive path fully establishes itself while the conductive blade forms a short circuit between the two distinct conductors inside the cable specimen. The bursts of arcing, when the current is non-zero, are clearly visible in both the 3D and the 2D spectrograms.

6.2.4 DC tests

The DC arc signal analysis starts with the test where PV panels are used as the power source and the steel wool with plastic tube is used as the arc initiator.

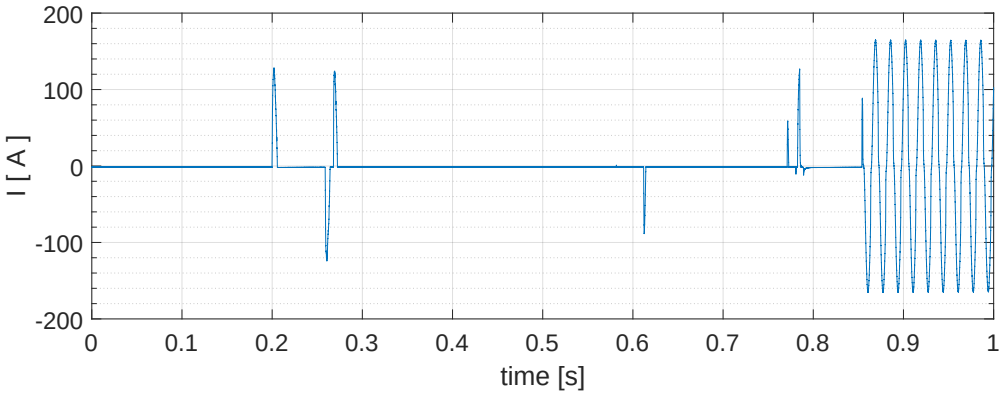

Fig. 6.40: Point contact test: Arc current

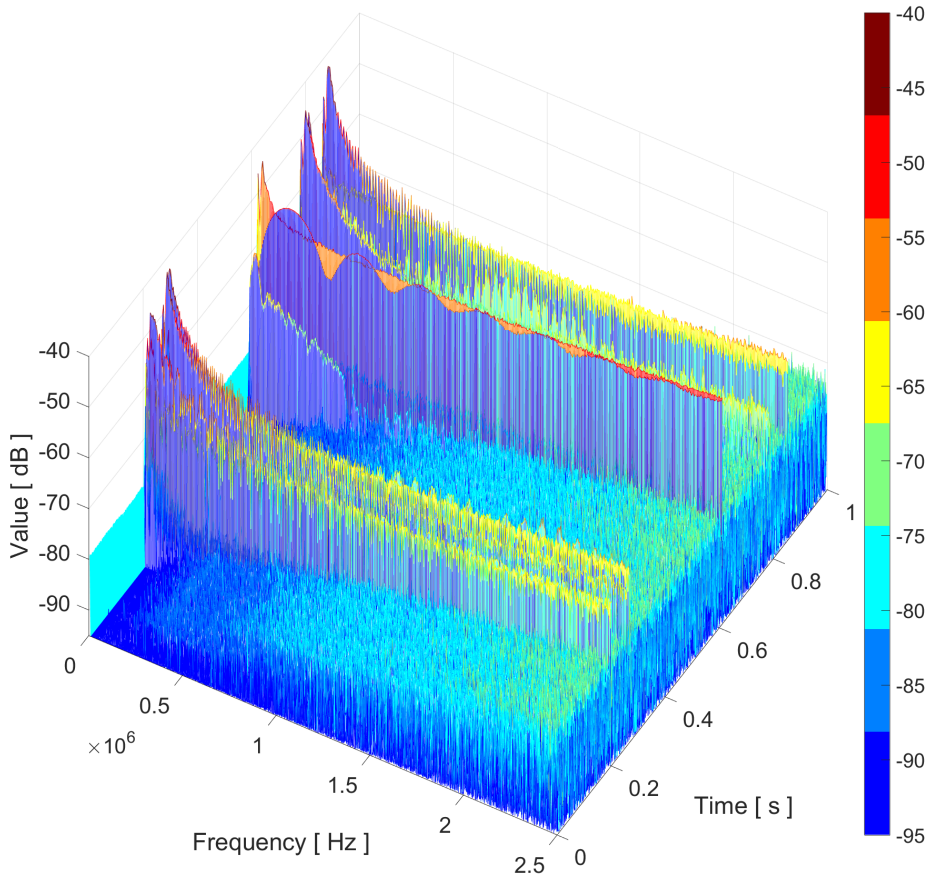

Fig. 6.41: The point contact test: The high-pass filtered arc current — a 3D spectrogram.

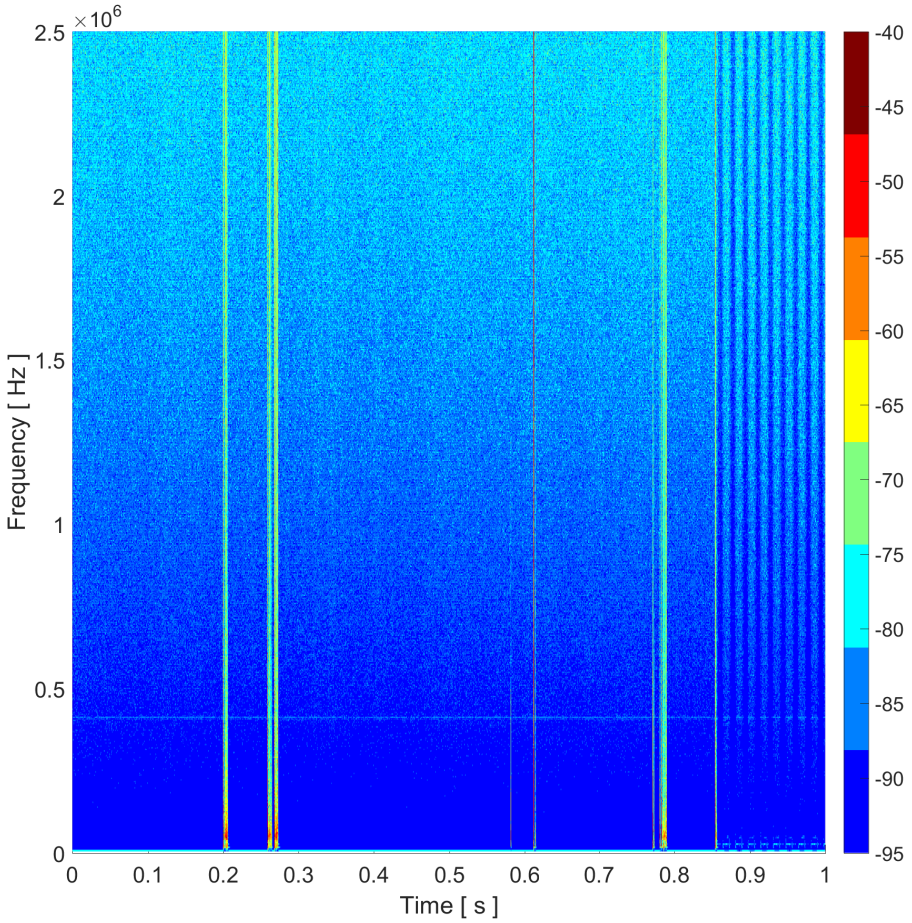

Fig. 6.42: The point contact test: The high-pass filtered arc current — a 2D spectrogram.

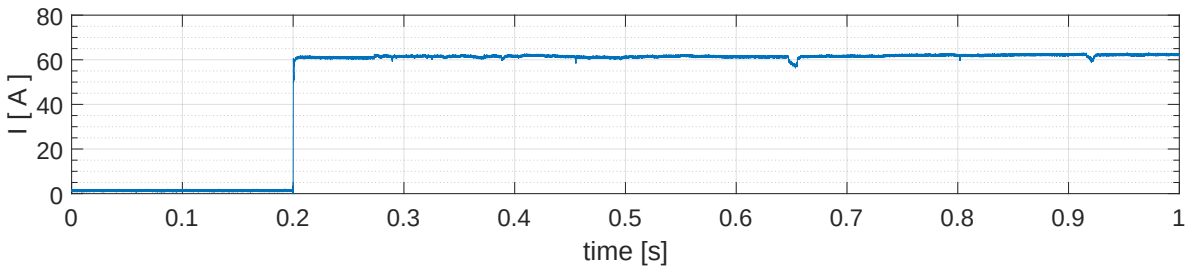

Fig. 6.43: The DC test: The arc current.

The circuit is energized and the arc is quickly ignited. The current with arc ignited remains rather stable with just a few minor changes in the current value, see Figure 6.43.

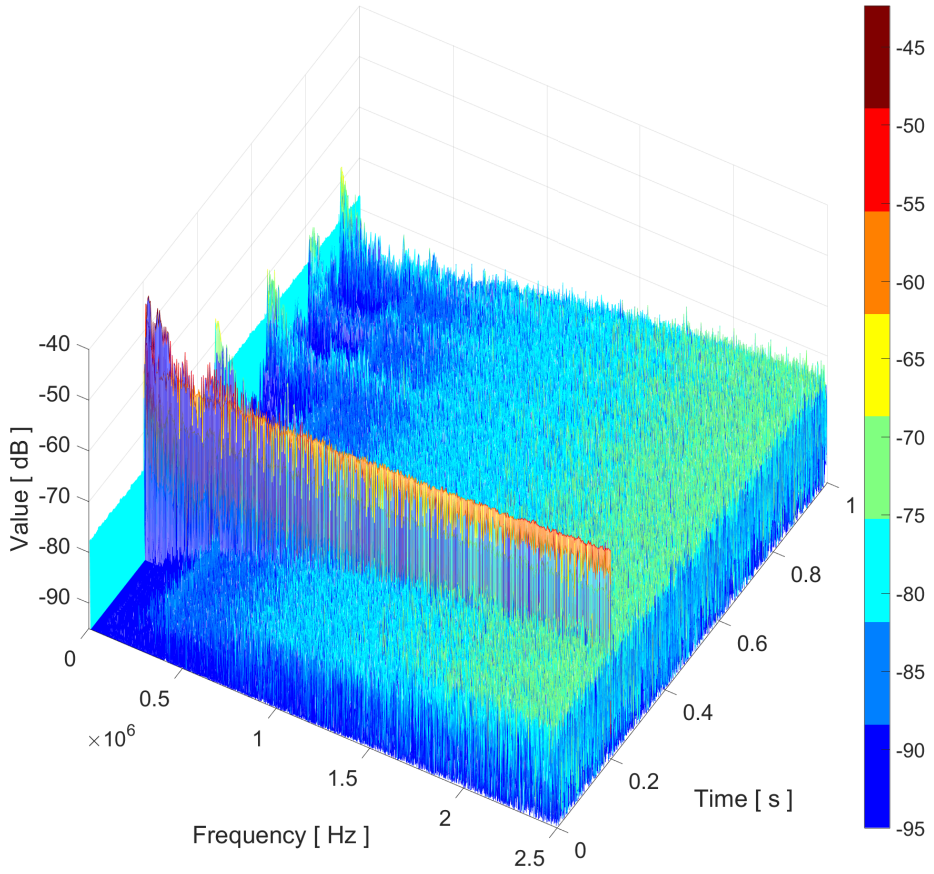

Fig. 6.44: The DC test: The high-pass filtered arc current — a 3D spectrogram.

The spectrogram shows that the repeated (periodic) broadband bursts typical of AC arcing are not present. On the other hand, the major broadband burst at $t = 0.2\ s$ clearly stands out in the 3D spectrogram, and several bursts with substantially lower energy (especially in the region below 1MHz) are also notable.

The arc-caused bursts are clearly visible in the 2D spectrogram plot (Fig. 6.45; we can see that the characteristic bursts are recognizable in the high-pass filtered signal spectrogram in the frequency range below 1 MHz.

6.2.5 DC test with the novel arc ignition procedure

The spectrograms for the springed wire test at the current level of 50 A with PV panels as the power source are almost completely noise-free (quiet), with merely some background noise signal of the source. The only two events distinguishable

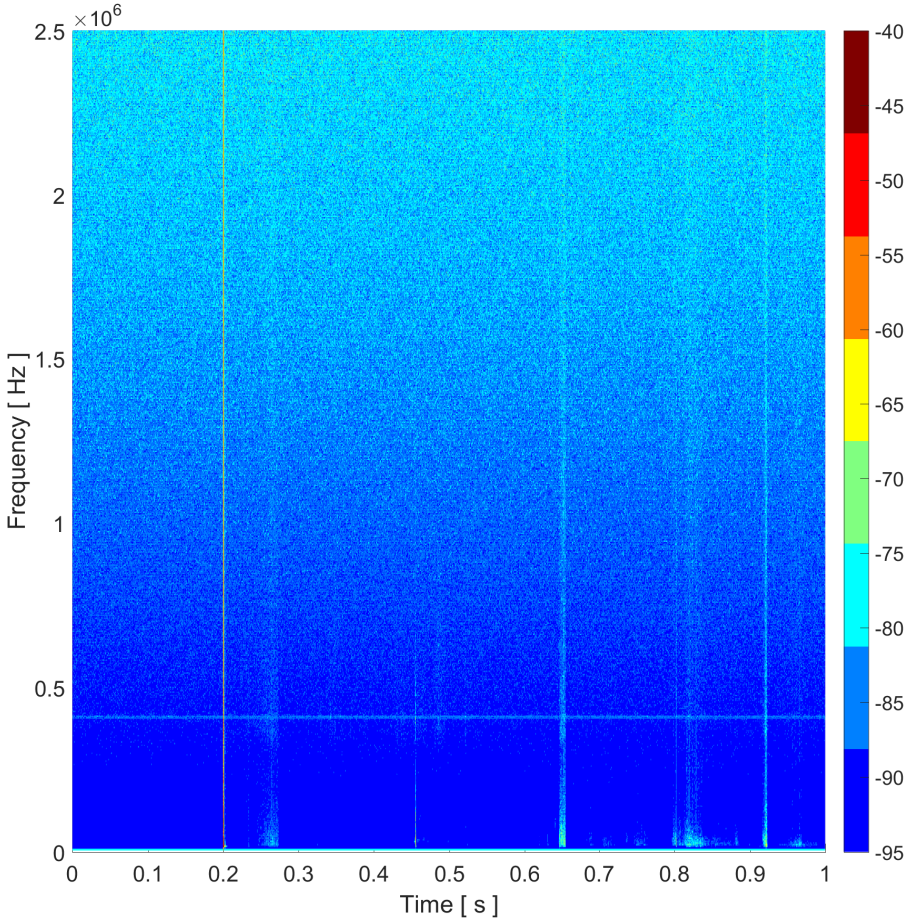

Fig. 6.45: The DC test: The high-pass filtered arc current — a 2D spectrogram.

here are the switching-on of the power source, and the rather noisy discrete ignition of the arc.

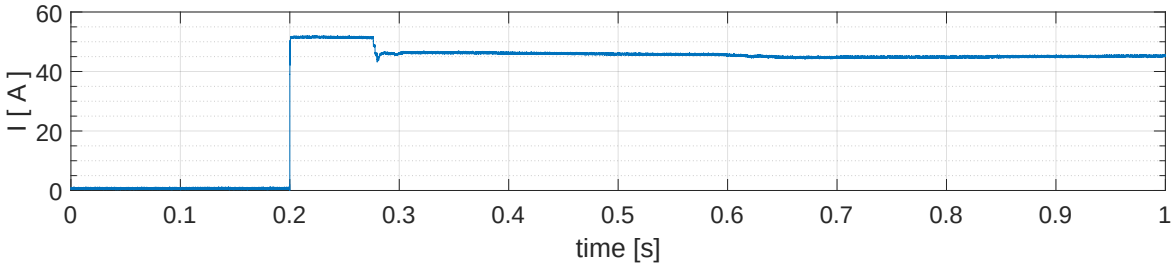

Fig. 6.46: The spring-based DC test: The arc current.

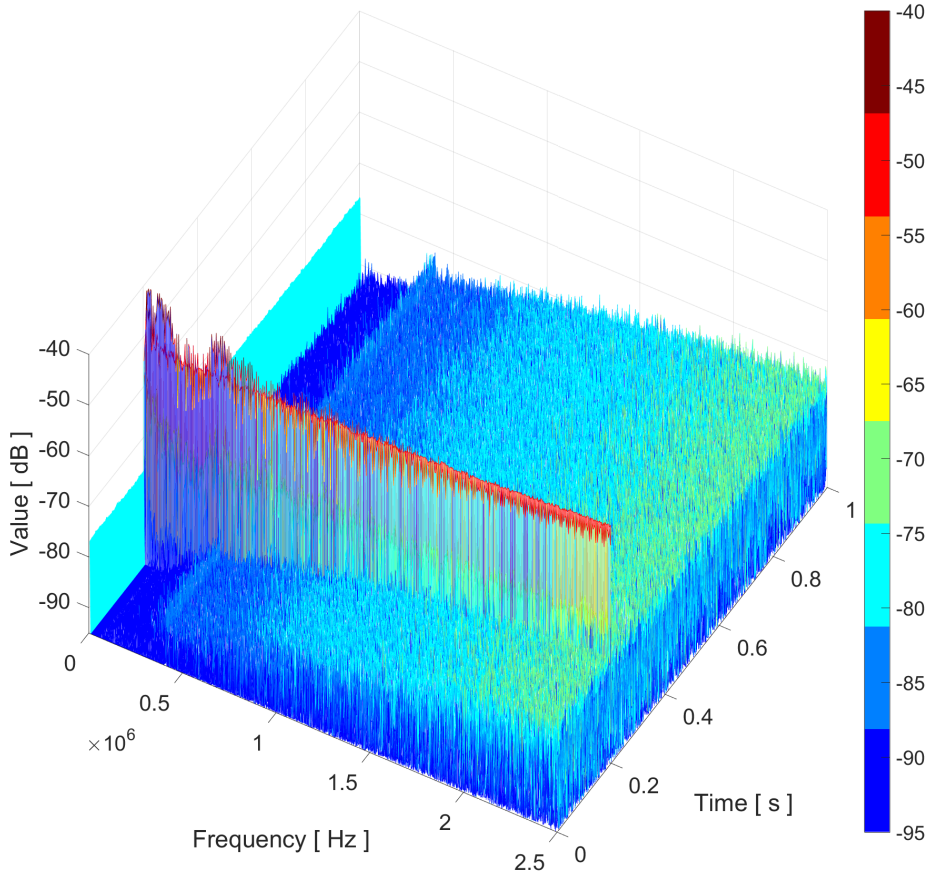

Fig. 6.47: The spring-based DC test: The high-pass filtered arc current — a 3D spectrogram.

The second spring test at the current level of 200 A, with a rectifier as the power source, is somewhat different from the previous one. The source itself emits more high- frequency noise; thus, the overall energy of the signal during the test is higher, and we can also observe the standing waves' peaks.

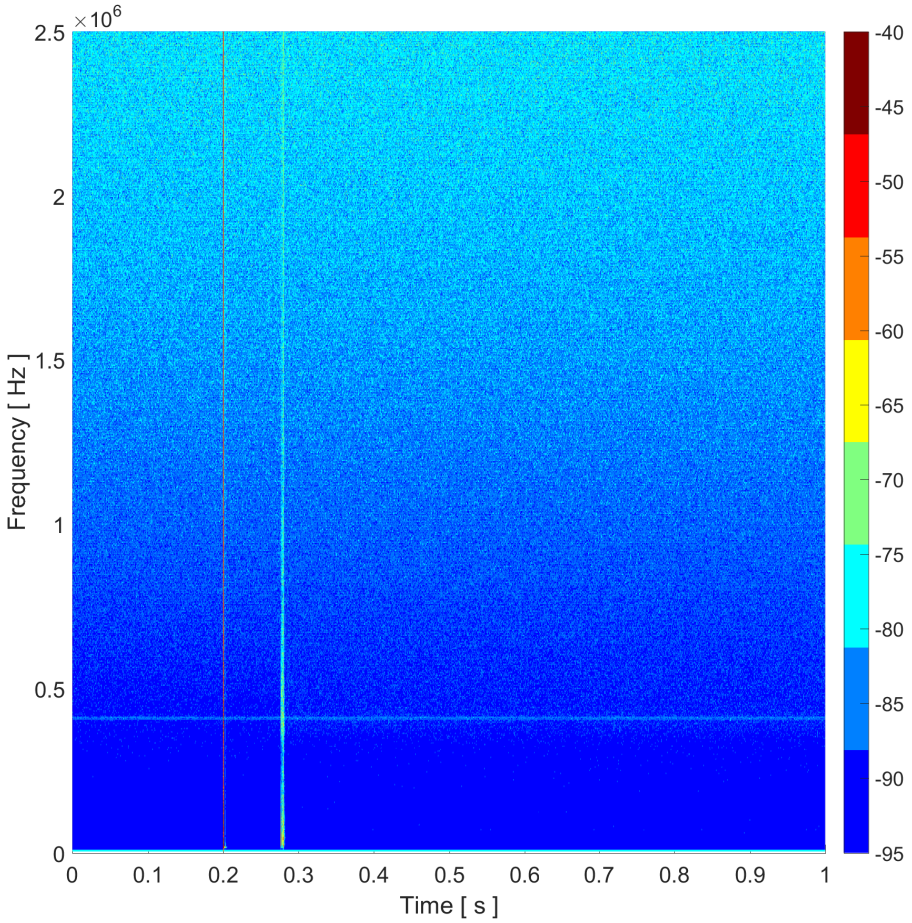

Fig. 6.48: The spring-based DC test: The high-pass filtered arc current — a 2D spectrogram.

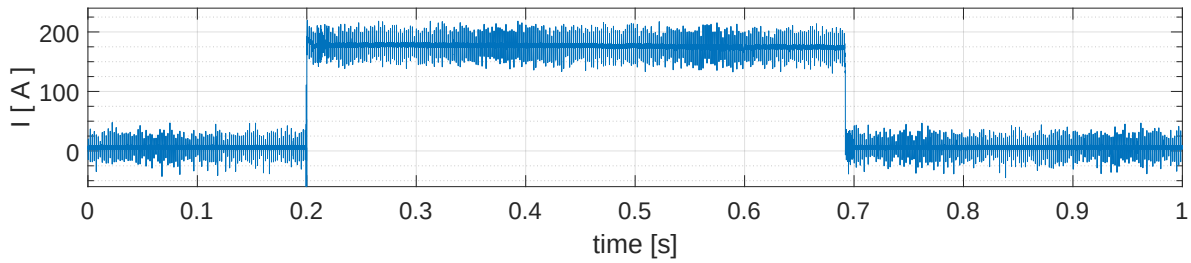

Fig. 6.49: The spring-based 200 A DC test: The arc current.

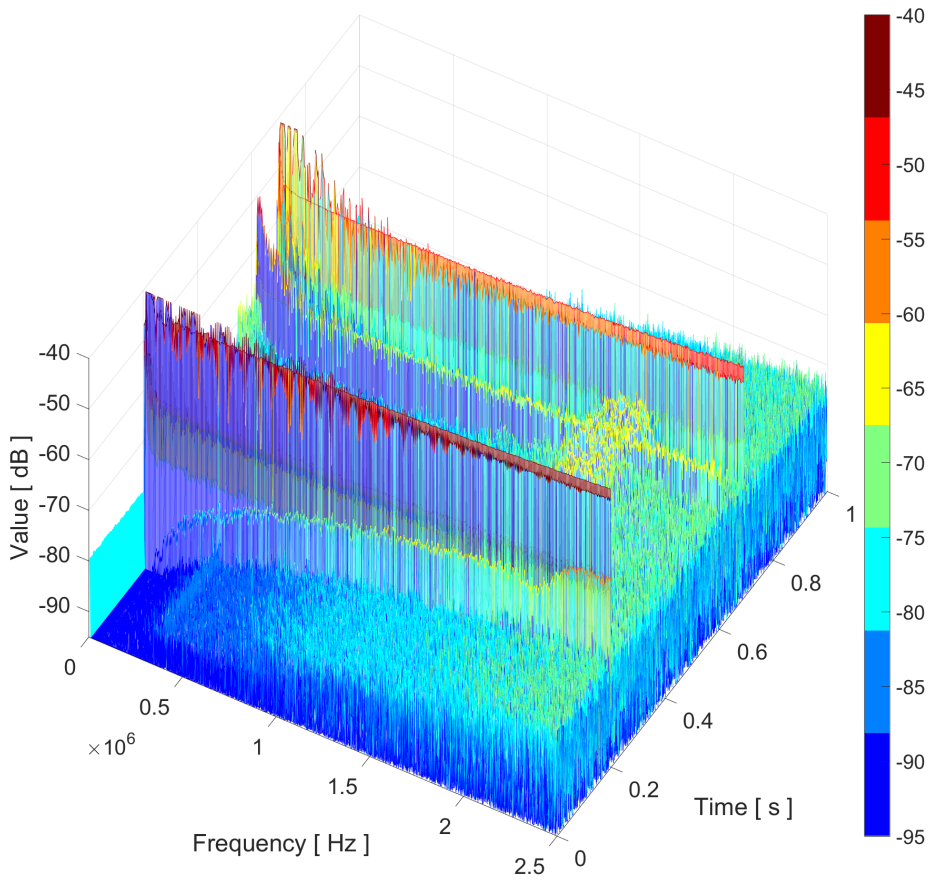

Fig. 6.50: The spring-based 200 A DC test: The high-pass filtered arc current — a 3D spectrogram.

In the 2D spectrogram, the broadband burst lines are clearly visible, standing out especially in the frequency band below 1 MHz, where the background high-frequency noise is relatively weak.

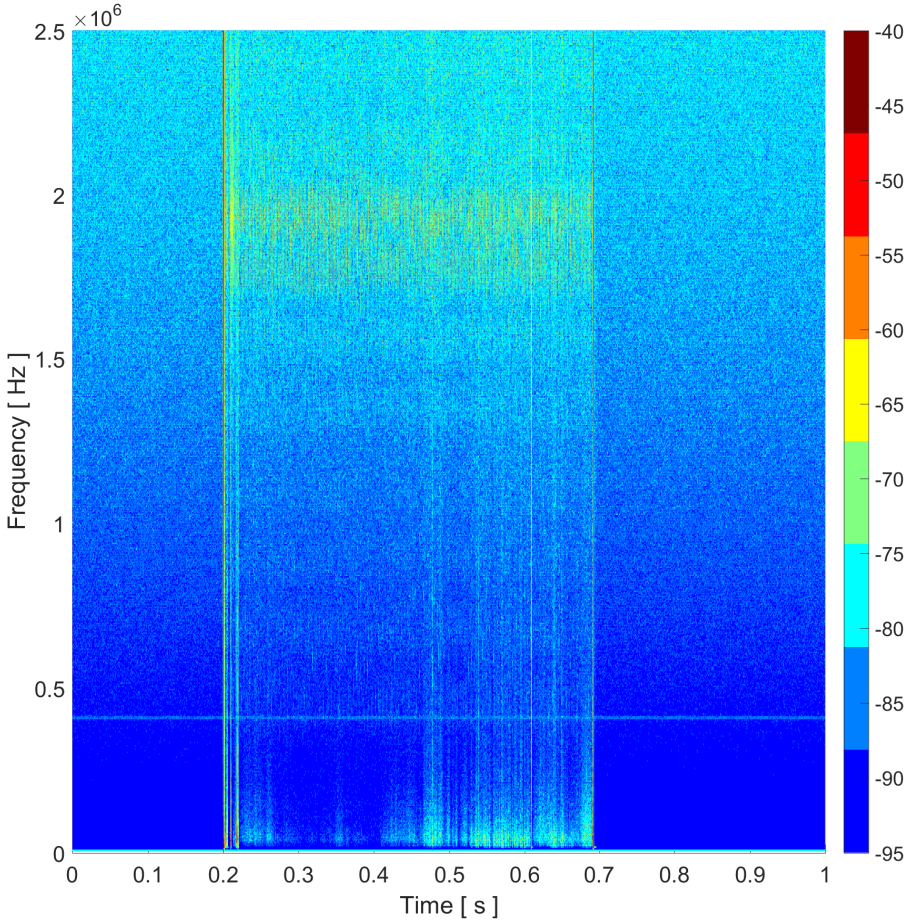

Fig. 6.51: The spring-based 200 A DC test: The high-pass filtered arc current — a 2D spectrogram.

6.3 Wavelet based analysis

In this chapter, we will focus on the wavelet transform as the last signal processing method used in this thesis. In this context, let us first compare the STFT used in the previous chapter to the wavelet transform, explaining why an additional tool for signal analysis is necessary. The authors of source [40] interpret the problem as follows:

> *"The short-time Fourier transform (STFT) is a time/frequency analysis technique which retains the time index of the frequency spectrum and seems to overcome the temporal localization problem. However, it still has a fundamental drawback in that the length of the window used in the STFT is the same for all frequencies. In order to obtain good frequency resolution, a large number of data points is required which in turn causes any short time variation within the window to be obscured on the resulting spectrum and minimizes the ability to temporally localize high frequency signals. If one wishes to have different resolutions in different parts of the frequency spectrum, the discrete STFT will have to be repeated for a number of window sizes. Thus, the problem is really that of time and frequency resolution tradeoff."*

For the time-frequency domain analysis of harmonic-related disturbances, it is possible to find the ideal window; however, the arc fault signature is distributed throughout many frequencies, and therefore finding an ideal window to obtain all information about the arcing event remains an unfeasible task.

6.3.1 Brief introduction to the Wavelet transform

The explanation above clarifies why even the STFT, despite being a useful tool, stops far from constituting an ideal instrument for the detection of arcing events. Nevertheless, additional signal processing methods are currently available in the mixed time-frequency domain. One of the more attractive techniques is signal analysis based on the wavelet transform; in our case, the discrete wavelet transform (DWT) will be used. A basic introduction to the principles of wavelet analysis is provided in [3]:

> *"Wavelet analysis is similar to Fourier analysis in the sense that it breaks a signal down into its constituent parts for analysis. Whereas the Fourier transform breaks the signal into a series of sine waves of different frequencies, the wavelet transform breaks the signal into its "wavelets", scaled and shifted versions of the "mother wavelet" ...*

. . . In contrast to the Fourier transform, the wavelet transform allows exceptional localization in both the time domain via translations of the mother wavelet, and in the scale (frequency) domain via dilations . . .

. . . The dilation function of the discrete wavelet transform can be represented as a tree of low and high pass filters, with each step transforming the low pass filter as shown in Figure. The original signal is successively decomposed into components of lower resolution, while the high frequency components are not analyzed any further.

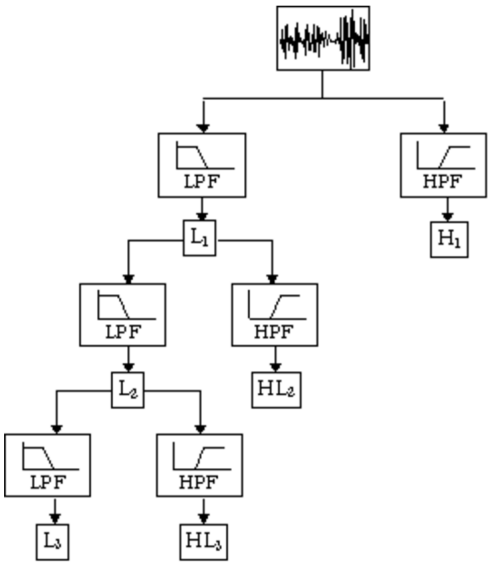

. . . The translation and dilation operations applied to the mother wavelet are performed to calculate the wavelet coefficients, which represent the correlation between the wavelet and a localized section of the signal. The wavelet coefficients are calculated for each wavelet segment, giving a time-scale function relating the wavelets correlation to the signal.“

The following pages present plots of wavelet coefficients for the same tests as were shown in the previous chapters. The mother functions applied were Coiflet 2, 3, 4, Daubechies 4, 5, 14, and Symlet 4, 5, 8.

6.3.2 Discrete wavelet transform-based analysis of AC test data

For both the AC and the DC signals, the data used as inputs for the wavelet transform are the 10 kHz high-pass filtered current data. In order to achieve better resolution, necessary in the DC signals, the data were transformed to a logarithmic scale before the wavelet transform was performed.

The mother functions listed above were evaluated for their ability to distinguish arcing events. Decomposition levels were tested up to level 12. For further presentation, this section will utilize coefficients obtained with the Coiflet 3 mother wavelet function at decomposition level 5. Wherever we consider it helpful to the reader, the current signal in the time domain will be displayed as well.

As regards the 60 Hz AC tests, the signals are very similar, enabling us to present and analyze them at once. In all of such signals, we can observe spikes of random height and duration at times when the transient events take place in the original signal. Because of the differences in the arcing for the different arc initiating methods, the presence of the spikes is different:

- The opposing electrodes test exhibits the spikes present during the whole arcing.
- The carbonated path test has short periods of the signal completely quiet.
- The point contact test shows only few high and well-distinguished spikes present in the signal.

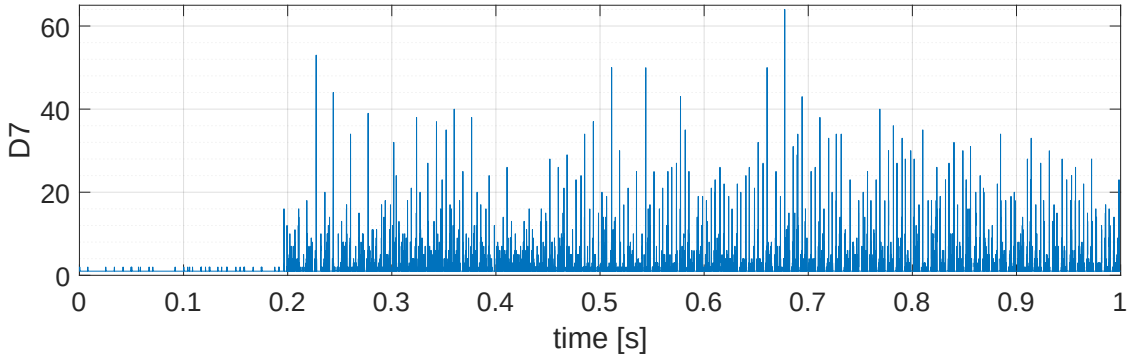

Fig. 6.52: The carbonated path test: Coiflet 3, decomposition level 7.

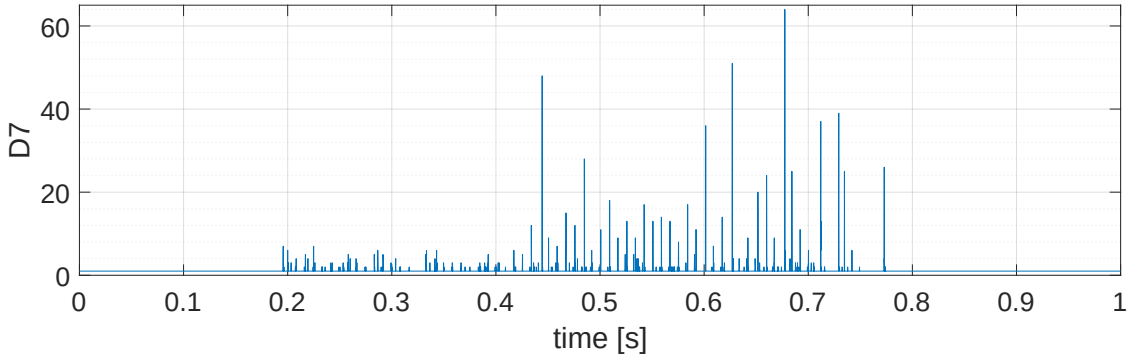

Fig. 6.53: The opposing electrodes test: Coiflet 3, decomposition level 7.

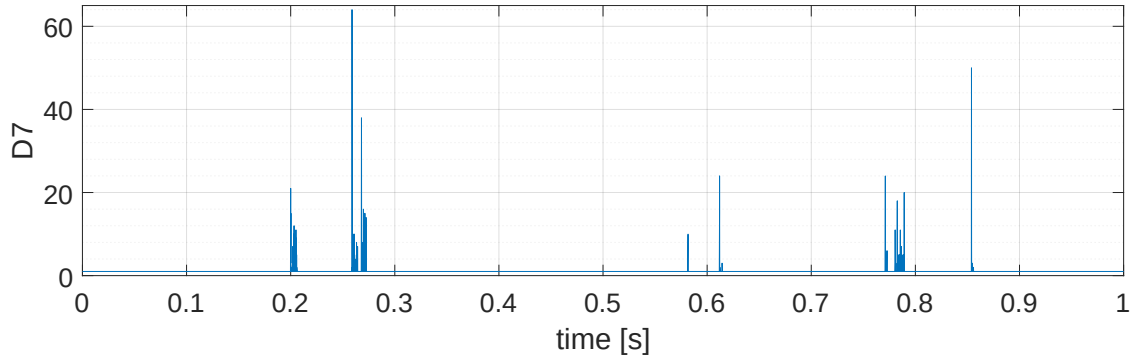

Fig. 6.54: The point contact test: Coiflet 3, decomposition level 7.

6.3.3 Discrete wavelet transform-based analysis of DC test data

As discussed in the previous chapters, looking for the arc signature is much more challenging in the DC arcing. To capture solely the arcing characteristics (arcing signature) without any additional load-related noise, the tests were carried on when the power sources (the PV panel, the Sorensen, and the custom-built DC source) were loaded with resistive loads only.

First, the PV panels' baseline test without arcing is displayed; it becomes obvious that the coefficients for the seventh decomposition of the signal significantly change only in the event of switching on the circuit. Otherwise, from the seventh decomposition level coefficients, it is not possible to distinguish whether the circuit is powered on or not. This satisfies our purposes because any further abrupt changes of the seventh decomposition level coefficients will be due to the arcing and the source.

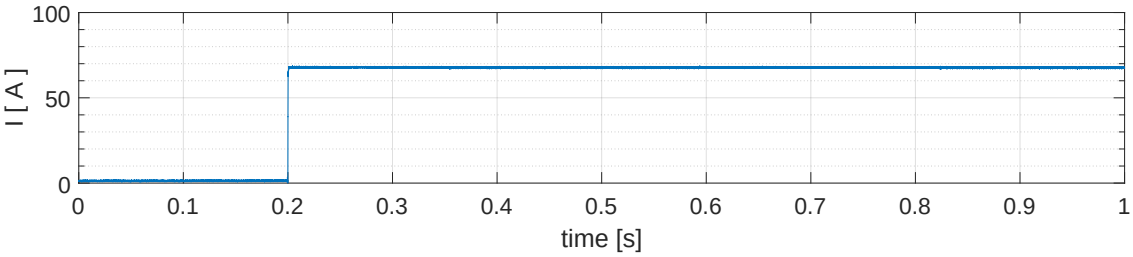

Fig. 6.55: The DC test baseline: the PV panels, 72 A.

The first arcing test displayed is the 72 A pre-arc test with steel wool and a plastic tube as the arc initiator and PV panels as the source. As the opposite of what was shown in the time and frequency domain chapters, here, while looking at the seventh decomposition level coefficients, we can clearly observe many spikes occurring randomly.

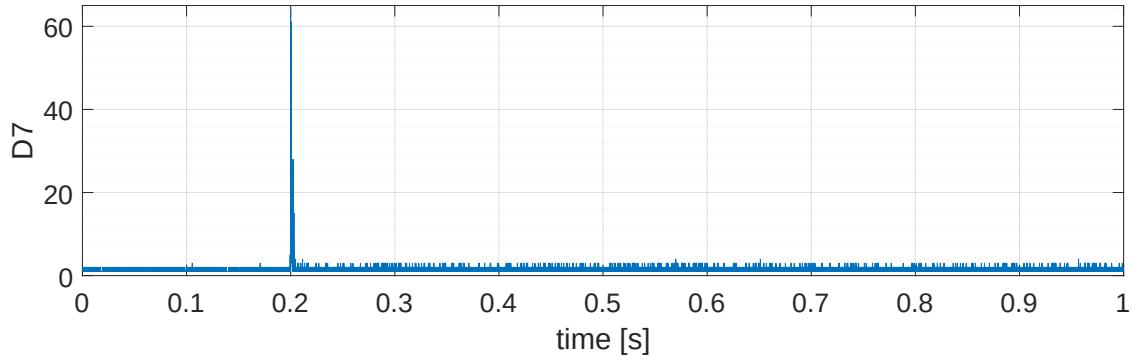

Fig. 6.56: The DC test baseline: the PV panels, 72 A: Coiflet 3, decomposition level 7.

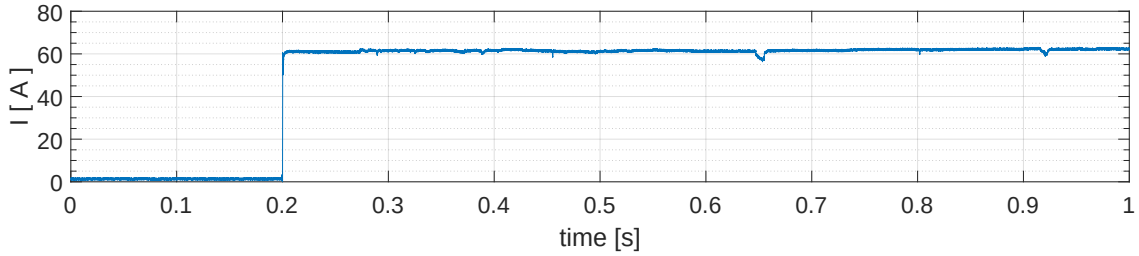

Fig. 6.57: The steel wool based DC test: the PV panels, 72 A.

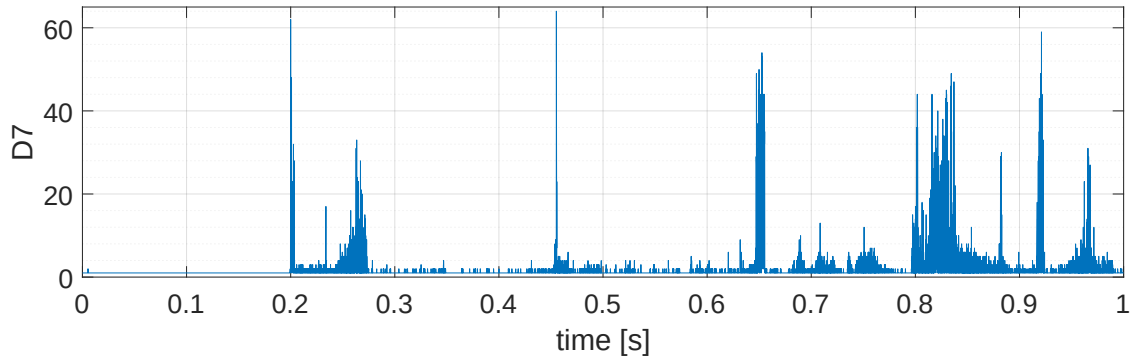

Fig. 6.58: The steel wool based DC test: the PV panels, 72 A: Coiflet 3, decomposition level 7.

The arc initiated by the applied steel wool held by a plastic tube exhibits physical properties different from those shown by the arc ignited with a springed wire; this is due to the carbon infused during the burning of the arc. For this reason, then, the signal characteristics of the tests differ significantly.

In the test with the arc initiated using a springed wire at 50 A, there were no significant features in the time and frequency domains that could be used to detect the arcing. However, in the case of the DWT, we can clearly observe switching the circuit on and off. The arc ignition is also openly detectable as we observe this event

in the form of a very high and broad spike, i.e., it consists of many individual spikes positioned next to each other. The most important feature for the arcing signature description is that the "base" signal present during the whole measurement doubles when the arcing is present. In other words, many very small transient events, which we were unable to observe in either the time or the frequency domains, are present in the signal during the arcing event. Taking advantage of the right mother wavelet function (Coiflet 3), we are then capable of detecting such events with the DWT.

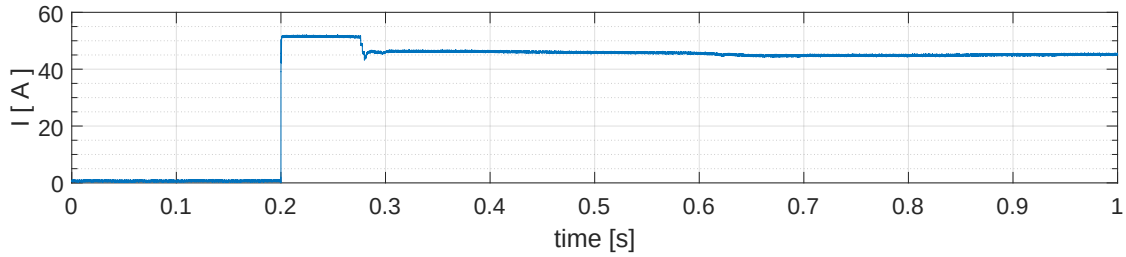

Fig. 6.59: The springed wire DC test: the PV panels, 50 A.

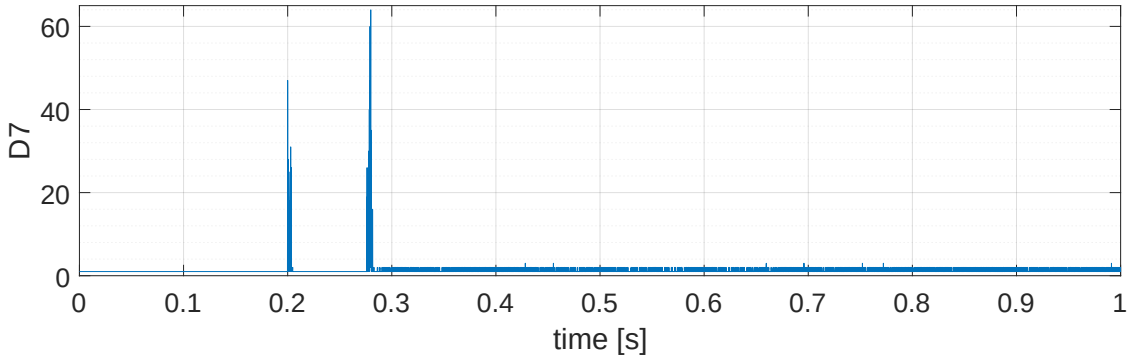

Fig. 6.60: The springed wire DC test: the PV panels, 50 A: Coiflet 3, decomposition level 7.

The second source used for the tests is the above-mentioned custom built DC source. The base signal test (no arcing) and its corresponding seventh decomposition level coefficients are shown below. In this case we may observe the circuit being switched on and off, but, apart from that, nothing else is noticeable.

The last test displayed below is the test with DC power supply with its signal baseline as shown in figures 6.61 and 6.62, the current is set to 200 A, but this time there will be arcing present. The arcing in this test is initiated with the springed wire.

As the current is very high, the arcing starts almost immediately after the circuit is closed. We cannot distinguish between powering the circuit up and the arc ignition. However, we have already acquired the seventh level coefficients for the source

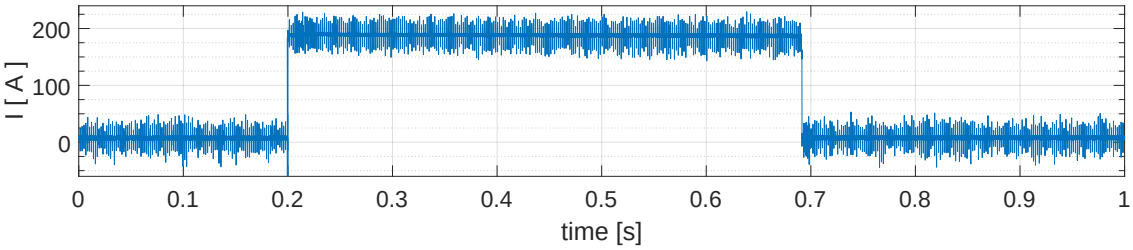

Fig. 6.61: The DC test baseline: the DC power supply, 200 A.

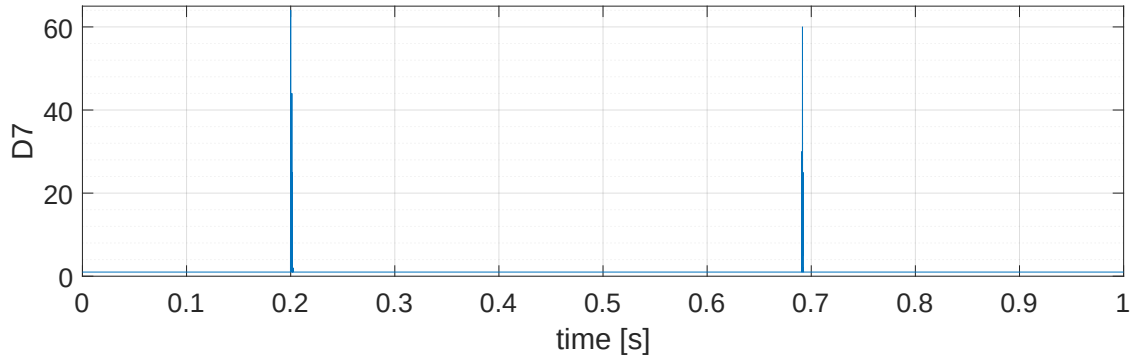

Fig. 6.62: The DC test baseline: the DC power supply, 200 A: Coiflet 3, decomp. level 7.

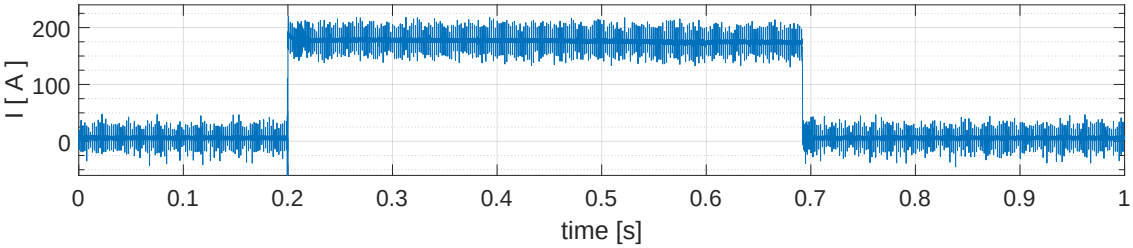

Fig. 6.63: The springed wire DC test: the DC power supply, 200 A.

operation without the presence of the arc (see figure 6.62 for reference), therefore we may conclude that the arcing is represented in the coefficients plot (figure 6.64) as spikes of random height positioned very densely across the whole arcing event.

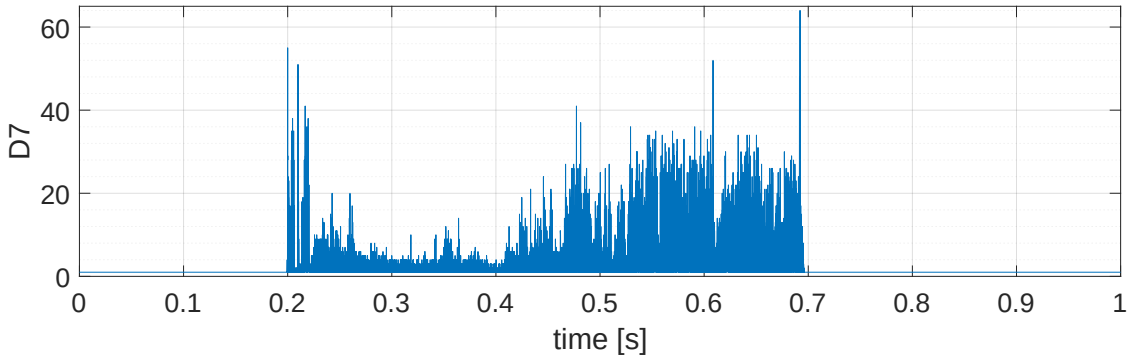

Fig. 6.64: The springed wire DC test: the DC power supply, 200 A: Coiflet 3, decomp. level 7.

7 PROPOSED DETECTION METHOD

In order to develop automated detection algorithm a method to perform the detection of events of interest has to be proposed. Arcing is an unpredictable event that has been found to affect subgroup of data rather than individual data points [29], therefore standard approaches to event detection can be applied. Basic general goals of event detection introduced in [29] are:

- Identify if an event of interest has occurred;
- Characterize the event (how is the subgroup of data affected);
- Detect as accurately as possible;
- Detect as early as possible.

In our case the early detection is required to minimize the energy dissipated by the electric arc to prevent fire ignition and/or heat-caused damage, while false positives (nuisance tripping) are highly undesirable due to economic factors. A trade off between early detection and false-positive detection probability has to be found. Therefore the detection algorithms has to have a tunable threshold to adjust detection sensitivity.

For the temporal event detection a uni-variate temporal methods are used as a relatively simple solution. General framework, according the the Event detection tutorial [29], is:

- Predict expected signal signal value.
- Measure difference between actual and expected signal values.
- Compute alarm value.

From the available uni-variate methods, methods based on moving averages like the Simple Moving Average (SMA), Weighted Moving Average (WMA), Exponentially Weighted Moving Average (EWMA) seem to be suitable candidate functions to characterize an actual signal value. Maximum expected signal value is the detection threshold. The event is detected either as soon as the moving average exceeds the threshold, or if the threshold remains exceeded for given amount of computational steps.

The SMA lets us compute an unweighted mean of the last n samples using a recursive formula [16]:

$$a_k = a_{k-1} + \frac{x_k - x_{k-n}}{n},$$

where a_k is a new value of SMA in step k, a_{k-1} is the SMA value computed in the previous step, x_k is the new sample in step k, n is the sliding window size and x_{k-n} is the oldest sample in the sliding window.

The Exponentially Weighted Moving Average (EWMA) averages the data in a way that gives less and less weight to data as they are further removed in time. By

selection of the weighting factor, α, the EWMA based detection sensitivity can be tuned as the parameter α determines how quickly the old data loose influence on the actual value of EWMA [30]. The EWMA is calculated as follows:

$$e_k = \alpha * x_k + (1 - \alpha) * e_{k-1},$$

where e_k is value of EWMA in step k, e_{k-1} is the EWMA value computed in the previous step, x_k is the new sample in step k and α is a forgetting parameter.

We observed that single arcing transient event lasted more than 5 ms, while switching related transient were shorter. Therefore our observation matches findings published in Chapter 4 State of the Art in the Arc-fault detection, where in the paper [14] the length of the time window was 10 ms.

If SMA is to be used, the window has to be significantly longer than the $5ms$, if EWMA is to be used, the α has to be set so that $5ms$ old data are not forgotten yet.

In general the threshold can be either fixed or adaptive. The adaptive solution presumes that during the installation there are no arcs, therefore the arc detection device can learn typical arc-free operation levels. In such a way the threshold level is tuned to local installation conditions at the time of installation.

7.1 Detection in time domain

From the signals presented, described and analyzed in Chapter 6 it is clear that the time domain signal processing is suitable for arcing detection in the AC domain only. Although researchers try to use time domain principles for the arcing detection in DC systems as well, which was documented in Chapter 4, in our case the time domain principles are not really useful as we need to detect arcing in circuits with higher power and high currents, i.e. the detection has to be really fast and reliable to prevent any damage.

In the case of the AC signals unfiltered current signal can be used for detection of flat parts of the signal around zero crossing. Extended part of flat signal near the zero crossing region is one of distinguishing features of arcing, however it is not truly exclusive feature as some loads are known to cause similar signal deformation. Additional sign of the arcing is that the current signal becomes very steep when the arc reignites. Computing di/dt and comparing it against a threshold value is additional mean of detection. By combining principles defined above (extension of flat parts above a threshold and evaluation of di/dt against a threshold) can be used to detect arcing in AC systems in the time domain.

7.2 Frequency domain

In the frequency domain detection of both AC and DC signals can be done. In both domains (AC and DC) we have observed the abrupt increase in the overall spectra (walls). In the case of DC signal the "walls" may be present only during the arc ignition, but nevertheless, they are always present and thus can be detected. As we have seen in Chapter 6 it is favorable to use high-pass filtered signal to minimize spectral leakage. Arcing events can be detected by performing the FFT for specified time window and computing the whole high-frequency energy of the signal. With the obtained energy value a simple moving average will be computed and compared to a threshold value.

7.3 Time-frequency domain

In Chapter 6, we demonstrated that the wavelet transform is a superior tool for the analysis and characterization of non-stationary signals. The ignition of an arc and arcing were found to be visually detectable using the wavelet transform for both the AC systems and the highly challenging DC systems.

In order to detect arcing via the advantageous use of the wavelet transform, the proposed method is to pre-process the signals (high-pass filtration and log-like transformation) as described in Chapter 6 and to perform the wavelet transform with a chosen mother wavelet (Coiflet 3) and decomposition level 7. The obtained coefficient values will be used as an input for the computation of the simple moving average. The arcing is detected by comparing the actual SMA value against a threshold.

8 CONCLUSION

It is well known that existing protection devices, including circuit breakers and RCBs, do not provide sufficient protection from arcing faults, even though undetected arcing may cause fires due to the extreme arc temperature. A brief fire statistics-based discussion in favor of the use of arc fault detection devices is provided in Chapter1. In Chapter 2 the AFDDs (Arc Fault Detection Devices) have been introduced and relations between relevant AFDD standards has been provided. Existing standard for residential AFDD have been provided and tests prescribed in those standards have been described. As the existing standards do not address emerging types of loads (loads that are based on high frequency switching power electronics generating HF noise) the existing AFDDs either may tend to trip excessively due to perceived electromagnetic noise or may not trip correctly as the electric arc symptoms are masked by the high frequency noise. This new challenges in the residential AC domain substantiate the need for novel robust arc detection methods.

Chapter 3 focuses on DC applications as with emerging high-current DC based systems (e.g. photovoltaics) arc fault detection solutions designed specifically for such DC applications are needed. The appropriate standard UL 1699B is described and it is shown, that this standard addresses only limited part of the PV. Protection systems for PV components where the current levels are between 100 A and 400 A and voltage levels are between 1000 V – 1500 V is also needed.

Chapter 5 describes measurements that were performed in Eaton laboratories in order to support development of novel arc detection method. As the AC grid measurements for European 50 Hz grid have already been available (provided by Eaton), the 60 Hz and DC measurements had to be performed. Complete series of UL 1699B tests have been done, additionally tests for higher currents up to 200 A have been performed.

During testing we observed that existing testing setup according to the UL standard is both inconvenient and insufficient for novel application areas. Therefore modification of the test setup leading to safer, more repeatable and more realistic measurements has been proposed. The innovative arc initiation procedure uses springed wire instead of steel wool. The new method was successfully applied and it was verified that this innovation solves drawbacks that were described in Chapter 5.1.1.

Chapter 6 focuses on analysis of the acquired data; time-domain based analysis and its inadequacy is described in Chapter 6.1. Signal analysis in the frequency domain based on Fourier transform is described in Chapter 6.2, Short-time Fourier transform (SFTF) and outcomes of its application on the acquired signal data is

described there. In spite of the fact that in order to analyze the non-stationary arc related signals the Frequency transform based tools are not ideal, in Chapter 6.2 is documented that using STFT it is possible to analyze and subsequently detect arcing in AC based systems. The Fourier transform based approach takes advantage of repeated (periodic) arc ignitions that are present in AC systems due to the zero-crossing nature of the AC power sources. From the analysis in this chapter it seems that sufficient information is available in the signal frequencies in between 10 kHz and 1 MHz therefore for the detection system based on Fourier transform sampling frequency of 2 MHz is sufficient. However, in this chapter it has also been documented that the SFTF seems to be an inadequate tool for DC based systems where periodic arc ignitions are not present.

In Chapter 6.3 Wavelet based analysis is introduced as a tool that enables to overcome time-frequency uncertainty constrain of the SFTF. Discrete wavelet transform (DWT) is used to analyze the AC and DC arcing signal data in the mixed time-frequency domain. Broad range of mother functions has been used in order to find mother function that makes reliable detection of arcing event possible. The *Coiflet 3* mother function has been found as the most suitable one. During the search for detection method based on DWT various decomposition levels up to the level 12 have been evaluated. The most reliable combination found for both AC and DC arcing was the Coiflet 3 mother function with decomposition level 7.

The proposed basic detection principle, which is described in 7, takes advantage of findings that were documented in Chapter 6. Detection methods that operate solely in time domain (for AC systems) and/or frequency domain (both AC and DC systems) are proposed.

However, for reliable and robust detection of the arcing events even in the challenging DC applications it is recommended to apply the high-pass filter on the current data in the pre-processing stage, perform log-like transform of signal data and then transform the data using the DWT — the proposed arc detection method is based on DWT with Coiflet 3 mother function. The arc is detected if the seventh level coefficients moving average exceeds a specific threshold.

BIBLIOGRAPHY

[1] EN 62606:2013 General requirements for arc fault detection devices (IEC 62606:2013 modified). CENELEC European Comittee for Electrotechnical Standardization, 2013.

[2] ČSN EN 62606 Obecné požadavky na obloukové ochrany. UNMZ, July 2014.

[3] Altmann, J.: Surfing the Wavelets: Wavelet Basics. Center of Machine Condition Monitoring, Monash University, Austrailia, 1996.
URL http://www.wavelet.org/tutorial/wbasic.htm

[4] Armijo, J., Kenneth Miguel; Johnson: Characterizing Fire Danger From Low Power PV Arc-Faults. In *Presentation at the 40th Photovoltaics Specilists Conference held June 8-13, 2014 in Denver, CO.*, 2014, s. 1–14.
URL http://www.osti.gov/scitech/biblio/1241765

[5] Arunachalam, S.; Diong, B.: A Parametric Model Approach to Arc Fault Detection for DC and AC Power Systems. In *Conference Record of the 2006 IEEE Industry Applications Conference Forty-First IAS Annual Meeting*, IEEE, 2006, ISBN 1-4244-0364-2, ISSN 0197-2618, s. 2249–2255, doi: 10.1109/IAS.2006.256855.
URL http://ieeexplore.ieee.org/lpdocs/epic03/wrapper.htm?arnumber=4025544

[6] BEAMA: The RCD Handbook: BEAMA Guide to the Selection and Application of Residual Current Devices. BEAMA Industrial and Single Phased Product Group, September 2010.
URL http://www.beama.org.uk/asset/7EE14AAB-81DB-4870-A9ACFBC5C58A94A2/

[7] Benedikt, O.: *Rozbor příčin požárů vzniklých v Jihočeském kraji v letech 2009 - 2013 od elektrických zařízení a návrh opatření ke zlepšení stavu.* Diplomová práce.Jihočeská univerzita v Českých Budějovicích, Zdravotně sociální fakulta, 2014.
URL http://theses.cz/id/ak8lpp/

[8] Bugra, A.: Spectral Leakage. Machine Learning Newsletter, sep 2012.
URL http://bugra.github.io/work/notes/2012-09-15/Spectral-Leakage/

[9] Cao, Y.; Li, J.; Sumner, M.; aj.: Arc fault generation and detection in DC systems. In *2013 IEEE PES Asia-Pacific Power and Energy Engineering*

Conference (APPEEC), IEEE, 2013, ISBN 978-1-4799-2522-3, s. 1–5, doi: 10.1109/APPEEC.2013.6837123.
URL http://ieeexplore.ieee.org/lpdocs/epic03/wrapper.htm?arnumber=6837123

[10] Digulescu, A.; Petrut, T.; Bernard, C.; aj.: Advanced signal processing techniques for detection and localization of electrical arcs. In *2014 10th International Conference on Communications (COMM)*, IEEE, 2014, ISBN 978-1-4799-2385-4, s. 1–4, doi:10.1109/ICComm.2014.6866749.
URL http://ieeexplore.ieee.org/lpdocs/epic03/wrapper.htm?arnumber=6866749

[11] Duan, P.; Xu, L.; Ding, X.; aj.: An arc fault diagnostic method for low voltage lines using the difference of wavelet coefficients. *2014 9th IEEE Conference on Industrial Electronics and Applications*, 2014: s. 401–405, doi:10.1109/ICIEA.2014.6931196.
URL http://ieeexplore.ieee.org/lpdocs/epic03/wrapper.htm?arnumber=6931196

[12] Faifer, M.; Ottoboni, R.; Rossi, M.; aj.: A method for the detection of series arc faults in DC aircraft power networks. *2013 IEEE International Instrumentation and Measurement Technology Conference (I2MTC)*, 2013: s. 778–783, doi:10.1109/I2MTC.2013.6555521.
URL http://ieeexplore.ieee.org/lpdocs/epic03/wrapper.htm?arnumber=6555521

[13] Gao, R. X.; Ruqiang, Y.: *Wavelets*. New York: Springer, 2010, ISBN 978-144-1915-443.

[14] Gao, Y.; Zhang, J.; Lin, Y.; aj.: An innovative photovoltaic DC arc fault detection method through multiple criteria algorithm based on a new arc initiation method. In *2014 IEEE 40th Photovoltaic Specialist Conference (PVSC)*, IEEE, 2014, ISBN 978-1-4799-4398-2, s. 3188–3192, doi:10.1109/PVSC.2014.6925613.
URL http://ieeexplore.ieee.org/lpdocs/epic03/wrapper.htm?arnumber=6925613

[15] Grichting, B.; Goette, J.; Jacomet, M.: Cascaded fuzzy logic based arc fault detection in photovoltaic applications. *2015 International Conference on Clean Electrical Power (ICCEP)*, 2015: s. 178–183, doi:10.1109/ICCEP.2015.7177620.
URL http://ieeexplore.ieee.org/lpdocs/epic03/wrapper.htm?arnumber=7177620

[16] Heindl, C.: Simple Moving Average. January 2010.
URL https://cheind.wordpress.com/2010/01/23/simple-moving-average/

[17] HSE: HSE Guidance Topics: The health and safety toolbox: How to control risks at work: Electrical safety. Health and Safety Executive, June 2014.
URL http://www.hse.gov.uk/toolbox/electrical.htm

[18] Jewett, J. W.; Serway, R. A.: *Physics for scientists and engineers with modern physics*. Melbourne: Brooks/Cole, Cengage Learning, 2010, ISBN 14-390-4875-4.

[19] Karter, M. J.: Fire Loss in the United States 2012. National Fire Protection Association, September 2013.
URL http://www.nfpa.org/~/media/files/research/nfpa-reports/overall-fire-statistics/fireloss2013.pdf?la=en

[20] Koziy, K.; Gou, B.; Aslakson, J.: A Low-Cost Power-Quality Meter With Series Arc-Fault Detection Capability for Smart Grid. *IEEE Transactions on Power Delivery*, 2013: s. 1584–1591, ISSN 0885-8977, doi: 10.1109/TPWRD.2013.2251753.
URL http://ieeexplore.ieee.org/lpdocs/epic03/wrapper.htm?arnumber=6502756

[21] Lathi, B. P.; Green, R.: *Essentials of digital signal processing*. New York: Cambridge University Press, 2014, ISBN 978-110-7059-320.

[22] Lezama, J.; Schweitzer, P.; Tisserand, E.; aj.: An embedded system for AC series arc detection by inter-period correlations of current. In *Electric Power Systems Research, vol. 129*, 2015, ISSN 03787796, s. 227–234, doi: 10.1016/j.epsr.2015.08.005.
URL http://linkinghub.elsevier.com/retrieve/pii/S0378779615002424

[23] Lezama, J.; Schweitzer, P.; Weber, S.; aj.: Arc fault detection based on temporal analysis. *2014 IEEE 60th Holm Conference on Electrical Contacts (Holm)*, 2014: s. 1–5, doi:10.1109/HOLM.2014.7031017.
URL http://ieeexplore.ieee.org/lpdocs/epic03/wrapper.htm?arnumber=7031017

[24] Li, D.; Song, Z.; Wang, J.; aj.: A Method for Residential Series Arc Fault Detection and Identification. *2009 Proceedings of the 55th IEEE Holm Conference on Electrical Contacts*, 2009: s. 8–14, doi:10.1109/HOLM.2009.5284428.

URL http://ieeexplore.ieee.org/lpdocs/epic03/wrapper.htm?arnumber=5284428

[25] Li, W.-J.; Li, Y.-C.: Arc fault detection based on wavelet packet. In *2005 International Conference on Machine Learning and Cybernetics*, IEEE, 2005, ISBN 0-7803-9091-1, s. 1783–1788 Vol. 3, doi:10.1109/ICMLC.2005.1527234.
URL http://ieeexplore.ieee.org/lpdocs/epic03/wrapper.htm?arnumber=1527234

[26] Ming, Z.; Tian, Y.; Zhang, F.: Design of arc fault detection system based on CAN bus. In *2009 International Conference on Applied Superconductivity and Electromagnetic Devices*, IEEE, 2009, ISBN 978-1-4244-3686-6, s. 308–311, doi:10.1109/ASEMD.2009.5306631.
URL http://ieeexplore.ieee.org/lpdocs/epic03/wrapper.htm?arnumber=5306631

[27] Naidu, M.; Schoepf, T.; Gopalakrishnan, S.: Arc fault detection scheme for 42-V automotive DC networks using current shunt. In *IEEE Transactions on Power Electronics*, issue 3, 2006, ISSN 0885-8993, s. 633–639, doi:10.1109/TPEL.2006.872385.
URL http://ieeexplore.ieee.org/lpdocs/epic03/wrapper.htm?arnumber=1629003

[28] Nan, C.; Yixing, T.; Qian, Z.: Experimental Research about the Current Characteristic of the Fault Arc in Series based on Wavelet Analysis. *Procedia Engineering,vol. 84*, 2014: s. 736–741, ISSN 18777058, doi:10.1016/j.proeng.2014.10.490.
URL http://linkinghub.elsevier.com/retrieve/pii/S1877705814018116

[29] Neill, D. B.; Wong, W.-K.: Tutorial on Event Detection KDD 2009. 2009, event and Pattern Detection Laboratory, H.J. Heinz III College, Carnegie Mellon University.
URL http://www.cs.cmu.edu/~neill/papers/eventdetection.pdf

[30] NIST: *NIST Engineering Statistics Handbook: Process or Product Monitoring and Control: Univariate and Multivariate Control Charts: What are Variables Control Charts?: EWMA Control Charts :*. NIST, 2015.
URL http://www.itl.nist.gov/div898/handbook/pmc/section3/pmc324.htm

[31] Restrepo, C. E.: Arc Fault Detection and Discrimination Methods. In *Electrical Contacts - 2007 Proceedings of the 53rd IEEE Holm Conference on Electrical Contacts*, IEEE, 2007, ISBN 1-4244-0837-7, s. 115–122, doi: 10.1109/HOLM.2007.4318203.
URL http://ieeexplore.ieee.org/lpdocs/epic03/wrapper.htm?arnumber=4318203

[32] Seo, G.-S.; Kim, K. A.; Lee, K.-C.; aj.: A new DC arc fault detection method using DC system component modeling and analysis in low frequency range. *2015 IEEE Applied Power Electronics Conference and Exposition (APEC)*, 2015: s. 2438–2444, doi:10.1109/APEC.2015.7104690.
URL http://ieeexplore.ieee.org/lpdocs/epic03/wrapper.htm?arnumber=7104690

[33] Siemens: History of the AFCI. Siemens Industry, Inc., 2012.

[34] Slade, P. G.: *Electrical contacts, Second edition.* Boca Raton: CRC Press, Taylor, 2014, ISBN 14-398-8130-8.

[35] Strobl, C.: Arc fault detection in DC microgrids. In *2015 IEEE First International Conference on DC Microgrids (ICDCM)*, IEEE, 2015, ISBN 978-1-4799-9880-7, s. 181–186, doi:10.1109/ICDCM.2015.7152035.
URL http://ieeexplore.ieee.org/lpdocs/epic03/wrapper.htm?arnumber=7152035

[36] UL: UL 1699 Standard for Safety: Arc-Fault Circuit Interrupters. UNDERWRITERS LABORATORIES INC., April 2006.

[37] UL: UL 1699B Outline for Investigation for Photovoltaic (PV) Arc-Fault Circuit Protection. UNDERWRITERS LABORATORIES INC., January 2013.

[38] Vrána, L.: Požární bezpečnost staveb z hlediska elektroinstalací. 2013.
URL http://www.pozarniodolnost.cz/docs/pdfs/Pozarni_bezpecnost_staveb_z_hlediska_elektroinstalaci_-_Brno_2013.pdf

[39] Wang, Z.; Balog, R. S.: Arc fault and flash detection in DC photovoltaic arrays using wavelets. In *2013 IEEE 39th Photovoltaic Specialists Conference (PVSC)*, IEEE, 2013, ISBN 978-1-4799-3299-3, s. 1619–1624, doi:10.1109/PVSC.2013.6744455.
URL http://ieeexplore.ieee.org/lpdocs/epic03/wrapper.htm?arnumber=6744455

[40] Wang, Z.; McConnell, S.; Balog, R. S.; aj.: Arc fault signal detection - Fourier transformation vs. wavelet decomposition techniques using synthesized data. In *2014 IEEE 40th Photovoltaic Specialist Conference (PVSC)*, IEEE, 2014, ISBN 978-1-4799-4398-2, s. 3239–3244, doi:10.1109/PVSC.2014.6925625.
URL http://ieeexplore.ieee.org/lpdocs/epic03/wrapper.htm?arnumber=6925625

[41] Xie, M.; Zhang, X.; Dong, Y.; aj.: Arc fault detection for DC Solid State Power Controllers. *2014 IEEE Conference and Expo Transportation Electrification Asia-Pacific (ITEC Asia-Pacific)*, 2014: s. 1–6, doi:10.1109/ITEC-AP.2014.6940864.
URL http://ieeexplore.ieee.org/lpdocs/epic03/wrapper.htm?arnumber=6940864

[42] Yao, X.; Herrera, L.; Wang, J.: A series DC arc fault detection method and hardware implementation. In *2013 Twenty-Eighth Annual IEEE Applied Power Electronics Conference and Exposition (APEC)*, IEEE, 2013, ISBN 978-1-4673-4355-8, s. 2444–2449, doi:10.1109/APEC.2013.6520638.
URL http://ieeexplore.ieee.org/lpdocs/epic03/wrapper.htm?arnumber=6520638

[43] Zhang, R.; Song, Z.: Arc Fault Detection Method Based on Signal Energy Distribution in Frequency Band. In *2012 Asia-Pacific Power and Energy Engineering Conference*, IEEE, 2012, ISBN 978-1-4577-0547-2, s. 1–4, doi:10.1109/APPEEC.2012.6307636.
URL http://ieeexplore.ieee.org/lpdocs/epic03/wrapper.htm?arnumber=6307636

LIST OF SYMBOLS, PHYSICAL CONSTANTS AND ABBREVIATIONS

A	Amper
a_k	Value of Simple Moving Average in step k
AC	Alternating Current
AFCI	Arc Fault Circuit Interrupter
AFDD	Arc Fault Detection Device
cm	centimeter
CWT	Continous Wavelet Transform
dB	Decibel
DC	Direct current
DFT	Discrete Fourier Transform
DWT	Discrete Wavelet Transform
e_k	Value of Exponentially Weighted Moving Average in step k
EMI	Electromagnetic Interference
EU	European Union
EWMA	Exponentially Weighted Moving Average
FFT	Fast Fourier Transform
FT	Fourier Transform
Hz	Hertz
I	Electric current
IEC	International Electrotechnical Commission
kHz	Kilohertz
MHz	Megahertz
mm	Milimeter

m	Meter
n	Length of the sliding window in SMA formula
N	Scaled measure
PV	Photovoltaic
RCB	Residual Circuit Breaker
RCD	Residual Current Device
S	Absolute sum
s	second
SMA	Simple Moving Average
STFT	Short Time Fourier Transform
THD	Total Harmonic Distortion
t	Time
USA	United States of America
USFA	United States Fire Administration
US	United States
U	Voltage
UV	Ultraviolet
VFD	Vacuum fluorescent display
V	Volt
W	Watt
WMA	Weighted Moving Average (WMA)
x_k	k^{th} data sample
α	Forgetting parameter in EWMA formula